CNS1-dependent regulatory T cells shape recovery from acute lung injury

Morgan J McCullough, Miriya K Tune, Jason W Griffith, Brianna L Banten, Minghong He, Yongqiang Feng, Benjamin G Vincent, J Justin Milner, Ageliki Tsagaratou, Yisong Y Wan, Hong Dang, Claire M Doerschuk, Jason R Mock

The Journal of Immunology, 2026, 215(5), vkag119
https://doi.org/10.1093/jimmun/vkag119
Research Article

CNS1-dependent regulatory T cells shape recovery from acute lung injury

Morgan J. McCullough[1,2], Miriya K. Tune[1,3], Jason W. Griffith[4,5], Brianna L. Banten[3], Minghong He[6], Yongqiang Feng[6], Benjamin G. Vincent[2,7,8], J. Justin Milner[2,7], Ageliki Tsagaratou[7,9], Yisong Y. Wan[2], Hong Dang[1], Claire M. Doerschuk[1,2,3,10,11], and Jason R. Mock[1,2,3,*]

[1]Marsico Lung Institute, UNC School of Medicine, University of North Carolina at Chapel Hill, Chapel Hill, NC, United States
[2]Department of Microbiology and Immunology, UNC School of Medicine, University of North Carolina at Chapel Hill, Chapel Hill, NC, United States
[3]Division of Pulmonary Diseases and Critical Care Medicine, Department of Medicine, UNC School of Medicine, University of North Carolina at Chapel Hill, Chapel Hill, NC, United States
[4]Center for Immunology and Inflammatory Disease, Massachusetts General Hospital, Harvard Medical School, Boston, MA, United States
[5]Division of Pulmonary and Critical Care Medicine, Massachusetts General Hospital, Harvard Medical School, Boston, MA, United States
[6]Department of Immunology, St. Jude Children's Research Hospital, Memphis, TN, United States
[7]Lineberger Comprehensive Cancer Center, UNC School of Medicine, University of North Carolina at Chapel Hill, Chapel Hill, NC, United States
[8]Division of Hematology, UNC School of Medicine, University of North Carolina at Chapel Hill, Chapel Hill, NC, United States
[9]Department of Genetics, UNC School of Medicine, University of North Carolina at Chapel Hill, Chapel Hill, NC, United States
[10]Department of Pathology and Laboratory Medicine, UNC School of Medicine, University of North Carolina at Chapel Hill, Chapel Hill, NC, United States
[11]Center for Airways Disease, UNC School of Medicine, University of North Carolina at Chapel Hill, Chapel Hill, NC, United States
*Corresponding author: Division of Pulmonary Diseases and Critical Care Medicine, Department of Medicine, University of North Carolina School of Medicine, Marsico Hall 7203, 125 Mason Farm Road, Chapel Hill, NC 27599, United States. Email: jason_mock@med.unc.edu

Abstract

Regulatory T cells (Tregs) play a crucial role in mediating recovery from acute lung injury (ALI). However, the complex roles of functionally heterogeneous Treg subsets in the lung during the resolution of acute inflammation remain unclear. To investigate the role of peripherally induced Tregs, we utilized mice lacking conserved noncoding sequence 1 (CNS1) of the *Foxp3* locus, a genetic deletion that impairs peripheral Treg induction. We found that CNS1-deficient mice exhibit greater mortality and delayed resolution during ALI. Tregs induced via CNS1 modulated antiviral and proinflammatory immune responses in the lung during influenza. Mechanistically, single-cell RNA sequencing reveals that CNS1-deficient Tregs fail to fully engage the Treg transcriptional program that supports optimal suppressive and reparative function in the lung. Our findings highlight a critical role for CNS1-dependent peripherally induced Tregs in determining ALI severity, providing insight into how distinct Treg subpopulations may be therapeutically harnessed to mitigate tissue damage during respiratory disease.

Keywords conserved noncoding sequence 1, CNS1, forkhead box P3, Foxp3, regulatory T cells, resolution of acute lung injury

Introduction

Regulatory T cells (Tregs) have been implicated in recovery from acute respiratory distress syndrome (ARDS) and murine models of acute lung injury (ALI).[1,2] Tregs are defined by the expression of the transcription factor Forkhead box protein 3 (Foxp3) and are necessary to maintain central immune tolerance,[3] as well as to modulate inflammation during tissue damage and infection.[1,2,4] Tregs increase in number in the lung following ALI, in which they regulate both the innate5–11 and adaptive12–15 immune response.[1,2] Tregs also mediate tissue repair processes by inducing the proliferation of type II pneumocytes (AT2 cells),[16,17] preventing fibrosis,[18] and facilitating angiogenesis[19] following ALI. Notably, Treg transcriptional heterogeneity has been reported, and lung Treg phenotypes change as ALI progresses.[5] In other models of lung infection, increases in Treg number have been found to be due to either the recruitment or induction of new Tregs at the site of infection.[20] These results indicate that Treg phenotypes are dynamic, but recent studies have not explored known *Foxp3* conserved noncoding sequences that may shape these phenotypes in ALI.

The respective roles of thymically derived Tregs (tTregs) and peripherally induced Tregs (pTregs) in resolution of ALI remain undescribed. tTregs are thought to express T cell receptors (TCRs) specific for self-antigens, which maintain central tolerance. In contrast, pTregs have TCRs specific for non–self-

Received: December 8, 2025. **Revised:** March 25, 2026. **Accepted:** April 6, 2026

antigens, such as those present in the host microbiome or diet, and function to maintain tolerance to these antigens in the gut.21–24 One mechanism of pTreg generation is via a conserved noncoding sequence in the *Foxp3* locus, conserved noncoding sequence 1 (CNS1).[25,26] When transcription factors such as SMAD (induced by TGF-β signaling)[27] and NFAT (induced by TCR signaling)[28] bind CNS1 in conventional $CD4^+$ T cells, *Foxp3* expression is induced.[29] Mice lacking CNS1 do not exhibit systemic autoimmunity but do have disrupted mucosal immunity,[21,26] indicating that pTregs arising via CNS1 have nonredundant roles in establishing tolerance at these sites. The role of pTregs induced via CNS1 in ALI remains unexplored.

Here, we study the pathogenesis of ALI in CNS1-deficient mice ($Foxp3^{\Delta CNS1-gfp}$ [ΔCNS1] mice).[25] The data show that ΔCNS1 mice exhibit heightened mortality in response to influenza-induced ALI, increased inflammation, and delayed resolution. Aberrant Treg phenotypes occur in ΔCNS1 mice, and several of these phenotypes persist in competitive chimeric environments. Mechanistically, we find that CNS1 is important for suppressing Th1 inflammation and inducing or maintaining a previously described tissue Treg subset.[5,8,10] Furthermore, CNS1 may play either a direct or indirect role in $CD4^+$ T cell polarization and the $CD4^+$ T cell response. Overall, these findings highlight a critical, nonredundant role for CNS1 in promoting tissue-specific Treg induction, fine-tuning immune regulation, and promoting resolution and repair in the lung after acute inflammation.

Methods

Mice

$Foxp3^{\Delta CNS1-gfp}$ mice[25] (ΔCNS1 mice) were a gift from Alexander Rudensky. C57BL/6J (wild-type [WT]) mice were obtained from the Jackson Laboratory (000664). *C57BL/6J-Ptprc*^{em6Lutzy}*/J* mice (JAXboy) were obtained from the Jackson Laboratory (033076). To generate mixed bone marrow chimera recipient mice, C57BL/6J mice were bred to JAXboy mice. *B6.129(Cg)-Foxp3*$^{tm3(HBEGF/GFP)Ayr}$*/J* (*Foxp3*^{DTR}) mice were obtained from the Jackson Laboratory (016958).[3] All mice were bred in-house at the University of North Carolina at Chapel Hill and maintained in specific pathogen-free facilities. The University of North Carolina at Chapel Hill Animal Care and Use Committee approved all procedures performed on animal subjects.

Initiation of inflammation by influenza

Male and female mice, 8 to 13 wk of age, were anesthetized with tribromoethanol, followed by intubation of the trachea and treatment with influenza A/PR/8/34 H1N1 (PR8) (Charles River; Catalog #10100374) as previously described.[30] In experiments with lower mortality rates (effective dose with approximately 20% mortality [ED20]), viral stocks were resuspended in phosphate-buffered saline (PBS) and stored at a concentration of 2×10^8 egg infectious dose/mL (EID) at −80 °C. Prior to intratracheal administration, PR8 stocks were diluted to 2.5×10^6 in PBS, and each mouse received 2 μL/g of body weight as previously described.[30]

In selective experiments eliciting higher mortality rates (ED40), a different PR8 stock from Charles River (Catalog #10100374) was diluted in PBS and stored at 2×10^8 EID at −80 °C. Prior to intratracheal administration, PR8 stocks were diluted to 6.25×10^4 EID/mL in PBS, and each mouse received 2 μL/g of body weight as previously described.[30] For chimeric experiments, a final dilution of 5×10^4 EID/mL in PBS was prepared from this stock.

Mice in all experiments were monitored daily following ALI induction by visual inspection and weighing, with the humane endpoint being reached when the mouse's weight dropped by more than 30% of the initial weight. Mice losing only ≥10% to 15% (depending on experiment) of the initial starting weight were included in the analysis.

All genotypes were analyzed in parallel except for selected experiments noted in relevant figure legends, which were processed 1 genotype at a time (1 independent experiment per genotype at days 4 and 10; 2 at day 15; sexes combined).

Pulse oximetry

Mice with shaved necks were monitored for blood oxygen saturation using the STARR MouseOx oximeter, collars, and software version 2.0.1.3.42.

Serum collection

Blood was collected via submandibular bleed with a 4 mm lancet (Braintree Scientific, Inc.) or postmortem by collecting the blood that pooled in the abdominal cavity following anterior vena cava severance with a pipette. Blood was collected in a serum separator tube (Fisher) and centrifuged at 6,000 *g* for 2 min. Serum that remained above the wax in the tube was aliquoted and stored at −80 °C until analysis.

Blood chemistry analysis

Alanine transaminase (SA1052), aspartate transaminase (SA1053), and creatinine (SA 1012) were measured by the Clinical Chemistry Core at the University of North Carolina at Chapel Hill using the Vet Axcel Chemistry Analyzer (Alfa Wassermann Diagnostic Technologies, LLC). Each test was calibrated and quality controlled directly prior to measurement using GEMCAL reference serum (S1-33), Level 1 Chemistry Control (C1-4), and Level 2 Chemistry Control (C1-5).

Lung morphology and scoring

Lung samples for histological analysis were prepared from study subjects by inflation to 25 cm H_2O with 10% neutral buffered formalin. Following fixation and dehydration, the lungs were embedded in paraffin wax and cut into 5 μm longitudinal sections. Lung sections were then stained with hematoxylin and eosin.

BAL analysis

Bronchoalveolar lavage (BAL) fluid was collected via intubation with a 20-gauge catheter, followed by 2 instillations of 0.7 mL of PBS and subsequent lavage. BAL cells and supernatants were centrifuged at 400 *g* for 5 min at 4° C. Supernatants were

removed and centrifuged at 1,300 *g* for 5 min at 4° C to remove debris, and the resulting supernatants were aliquoted and stored at −80° C for future analysis. Total protein was determined with the DC Protein Assay Kit (Bio-Rad). Cell pellets were treated with ACK lysis buffer (Gibco) at room temperature for 1 min, followed by the addition of PBS and centrifugation at 400 *g* for 5 min at 4 °C. BAL cells were then resuspended in PBS (0.25 mL) and counted using a hemocytometer with trypan blue exclusion. In some experiments, BAL cells were analyzed via flow cytometry (see the following).

Cytokine analysis of the BAL fluid was performed using the Bio-Plex Pro Mouse Cytokine 23-plex Assay (Bio-Rad).

Mixed bone marrow chimeras

Mixed bone marrow chimera mice were generated by irradiating C57BL/6J × JAXboy mice (Cesium-137 irradiator, 9 Gy) 1 d prior to retro-orbital adoptive transfer of 5 million splenocytes and 10 million bone marrow cells, with equal contributions coming from WT and ΔCNS1 mice. Chimeras were donor-recipient sex matched. Recipient mice were treated with ad libitum sulfamethoxazole/trimethoprim oral suspension (200 mg/40 mg per 5 mL) diluted in drinking water for 2 wk. Mice were analyzed 8 to 10 wk following bone marrow reconstitution (naïve mice) or treated with PR8 as described previously, 8 wk following reconstitution for day 10 or day 15 analysis.

Single-cell suspension preparation

In some experiments, mice were treated intravenously (retro-orbitally) with 0.1 mL of 0.03 mg/mL anti-mouse CD45 BV785 (BioLegend) 3 min prior to sacrifice.

Lungs

Mouse lungs were digested as previously described.[30] Briefly, the trachea was cannulated with a 20 g catheter, and perfusion via the right ventricle with 2 mL of 1× PBS was performed. Lungs were instilled with 1 mL of digestion buffer (5 mg/mL collagenase I [Worthington Biochemical] and 0.25 mg/mL DNase I [Sigma-Aldrich] in RPMI 1640 media [Life Technologies]). Then, 0.5 mL of 1% low-melting-point agarose (Invitrogen) was instilled. After agarose solidification, the lungs and heart were extracted and isolated. They were then incubated for 20 min at 37 °C and 5% CO_2 in a 12-well plate preloaded with 0.5 mL of the digestion buffer described previously. The lungs were then mechanically disrupted by passing them through a 16- or 18-gauge needle (kept constant across experiments). Resuspended lungs were then passed through a 100 μM filter and rinsed with 10 mL FACS buffer (PBS with 1% bovine serum albumin [BSA] and 2 mM EDTA). Cells were then centrifuged at 400 *g* for 5 min at 4 °C. Red blood cells in the cell pellet were lysed with 0.8 mL ACK lysis buffer (Gibco), the reaction was quenched with 5 mL FACS buffer, and cells were centrifuged at 400 *g* for 5 min at 4 °C. Total lung cells were quantified via a hemocytometer with live/dead exclusion.

Spleens

Mouse spleens were harvested and stored in at least 1 mL of RPMI media (Life Technologies). Single-cell suspensions were prepared by grinding spleens through a 40 μM filter, followed by rinsing with 10 mL RPMI 1640. Cells were then centrifuged at 400 *g* for 5 min at 4 °C. Red blood cells were lysed with ACK lysis buffer (Gibco), the reaction was quenched with FACS buffer, and cells were centrifuged at 400 *g* for 5 min at 4 °C. Splenocytes were resuspended in 0.5 mL FACS buffer, and total splenocytes were quantified via a hemocytometer with live/dead exclusion.

Flow cytometry

All preparation steps prior to analysis were performed on ice. A total of 1.5×10^6 cells (lungs, spleens) and half of total BAL cells were treated with rat anti-mouse CD16/32 (Fc block; BioLegend) for 5 min. Cells were then treated with surface antibodies, followed by fixation with the Foxp3/Transcription Factor Staining Buffer Set (eBioscience) and intracellular staining.

For some experiments, lung and spleen cells were activated with a Cell Activation Cocktail containing phorbol-12-myristate 13-acetate (40.5 μM), ionomycin (660.3 μM), and brefeldin A (2.5 μg/mL) in dimethyl sulfoxide (BioLegend) for 6 h at 37 °C and 5% CO_2. Cell Activation Cocktail dilutions were prepared by adding 2 μL Cell Activation Cocktail per 1 mL lymphocyte medium (see the following), and 3×10^6 cells were activated in 1 mL of Cell Activation Cocktail dilution in a 12-well tissue culture plate. Following activation, cells were collected and washed in FACS buffer. Activated cells were then stained as described previously for surface markers, cytokines, and other secreted effector molecules.

For some experiments, the reactivity of $CD4^+$ or $CD8^+$ T cells to a common PR8 antigen was assessed using tetramers prepared by the National Institutes of Health Tetramer Core. Tetramer staining was performed by incubating lung or spleen cells in a 96-well plate (1.5 million cells/well) in 200 μL of lymphocyte medium (see the following) and 1 μL of tetramer or isotype. Cells were incubated at 37 °C and 5% CO_2 for 1 h. Cells were then centrifuged at 400 *g* for 5 min at 4 °C, followed by resuspension of cells in 100 μL FACS buffer and recentrifugation at 400 *g* for 5 min at 4 °C. Cells were then resuspended in Fc block diluted in FACS buffer, and surface and intracellular staining proceeded as described previously.

All antibodies used in flow cytometry analyses are listed in Table S1. Following staining, cells were analyzed using a Cytoflex flow cytometer (Beckman Coulter) and associated CytExpert software, version 2.5 (Beckman Coulter).

Lymphocyte medium

Lymphocyte medium constitutes 10% fetal bovine serum, 2 mM L-glutamine, 1 mM sodium pyruvate, 100 mM nonessential amino acids, 5 mM HEPES, and 100 U/mL penicillin-streptomycin.

Treg purification for single-cell RNA sequencing analysis

To enrich lung samples for Tregs, we combined chimeric lung samples and created single-cell suspensions as described previously. Lung cells were then enriched for lymphocytes via a 33.3% Percoll density gradient medium (Cytiva), followed by

Treg isolation with a $CD4^+CD25^+$ Regulatory T cell Isolation Kit (Miltenyi Biotec). Purified cells were stored in Cryostor (Sigma-Aldrich) in liquid nitrogen prior to analysis.

Hemagglutinin-specific ELISA

The 96-well ELISA plates (Ancillary Reagent Kit; R&D Systems) were coated with inactivated recombinant H1N1 PR/8 hemagglutinin (HA) protein diluted to 3 μg/mL in bicarbonate buffer (Sigma-Aldrich), and 0.1 mL per well was loaded into each well. The plate was covered with film and incubated at 4 °C overnight. The plate was then washed 3 times with wash buffer (1× PBS) using a plate washer and blocked with blocking buffer (3% BSA in 1× PBS) at room temperature for 2 h. Washing was repeated, followed by incubation with samples and standards. The capture antibody in the Influenza A H1N1 Hemagglutinin/HA Pair Set served as the standard for this assay. This antibody was diluted to 30 μg/mL in reagent diluent (3% BSA in 1× PBS) for the highest standard, and then further diluted 1:4 for subsequent standards. Serum samples were run at 10^{-2}, 10^{-3}, 10^{-4}, and 10^{-5} dilutions. BAL samples were run neat, then at 10^{-1}, 10^{-2}, and 10^{-3} dilutions. Samples were diluted in the reagent diluent. Samples were incubated at room temperature for 2 h, then washed as described previously. Detection antibody (anti-IgG HRP, company) was diluted 1:10,000 in reagent diluent, and 100 μL was added to each well, incubated for 2 h at room temperature. The plate was then washed and developed with ELISA substrate solution (Ancillary Reagent Kit), which was added at 100 μL per well and incubated for 20 to 30 min in the dark, or until the assay was developed. Development was stopped with a substrate solution (Ancillary Reagent Kit), and then the well absorbance was read with a plate reader (Bio-Rad) at 450 nm.

Immunoglobulin subtyping

Immunoglobulin subtyping was performed with the LEGENDplex Mouse Immunoglobulin Isotyping Panel (6-plex) with V-bottom Plate (BioLegend) following the manufacturer's instructions. BAL samples were diluted 1:128 (naïve) or 1:256 (day 10 and day 15 post-PR8). Samples that were out of range were not reported and were excluded from analysis.

Autoantibody array

Serum samples from naïve, day 11 post-PR8, and day 15 post-PR8 were analyzed by the University of Texas Southwestern Microarray and Immune Phenotyping Core using previously described methodology.[31] Naïve serum was isolated via submandibular cheek bleed, and day 11 and 15 serum were isolated from blood collected from the abdomen following inferior vena cava severance. The data presented in the heatmaps are normalized signal intensities. Antigens were removed from analysis if they had a >10% signal-to-noise ratio >3.

$CD4^+$ adoptive transfer studies

For the adoptive transfer studies involving donor cells obtained from naïve *Foxp3*^{DTR} mice 50 million splenocytes were isolated delivered retro-orbitally to WT recipient ($CD45.1^+$ $CD45.2^+$) mice. Then at 24 and 48 h post–adoptive transfer, diphtheria toxin (1.25 μg) was delivered intraperitoneally to deplete any *Foxp3*^{DTR} Tregs present in the transferred splenocytes. After diphtheria toxin administration, PR8 induced lung injury was induced and we examined Foxp3 expression specifically in transferred $CD45.2^+$ $CD4^+$ cells 15 d post-PR8 in the recipient ($CD45.1^+$ $CD45.2^+$) mice.

For the adoptive transfer studies involving either ΔCNS1 or *Foxp3*^{DTR}, $CD4^+$ $CD25^-$ donor cells were obtained from the lungs or spleen of mice at 8 d post-PR8. $CD4^+$ $CD25^-$ cells were isolated after removal of Tregs using the Treg isolation kits as described previously. The $CD4^+$ $CD25^-$flow-through cells were delivered retro-orbitally to ΔCNS1 mice (2 million cells) that had been preinfected with PR8 on the same day. One day after adoptive transfer, diphtheria toxin (1.25 μg) was delivered intraperitoneally to deplete any WT Tregs that may have been present in the $CD4^+$ flow-through adoptively transferred sample.

ΔCNS1 and *Foxp3*^{DTR} studies

For the ΔCNS1 × *Foxp3*^{DTR} heterozygote studies, ΔCNS1 × *Foxp3*^{DTR} and JAXboy × *Foxp3*^{DTR} female F1 mice were treated with diphtheria toxin (0.25 μg) every day from 2 d prior to PR8 treatment to day 15 post-PR8, excluding the day of PR8 treatment.

Single-cell RNA sequencing analysis

Cells were sent frozen to Azenta Life Sciences, where they were frozen until the time of analysis. TotalSeq antibodies (BioLegend) were applied to cells according to the manufacturer's guidelines. Cells were then processed with the Chromium X, and single-cell RNA libraries were made with Chromium Next GEM Single Cell 5′ Kit with Feature Barcoding and the Chromium Single Cell Human BCR Amplification Kit for V(D)J library preparation. Quality was assessed before using the Illumina sequencing platform conFig.d to 10x Genomics recommendations. Data generated with the Illumina sequencing platform were converted to FASTQ files and de-multiplexed. Gene expression, VDJ, and CD45 barcoding data were integrated using the Cellranger multi command and a mouse reference genome.

The raw sequence files in FASTQ format were preprocessed using the Cell Ranger v8.0.1 (10x Genomics) pipeline in multi-mode, with GEX, TCR-VDJ, and antibody CITE-seq libraries. The cellranger outputs were further processed with workflows built with R libraries, *decontX*[32] for ambient RNA and background antibody decontamination and *scDblFinder*[33] for doublet removal, and the barcodes were filtered to retain cells with >300 gene counts and <10% mitochondrial transcripts using *Seurat.*[34] Antibody-derived tags against CD45.1 and CD45.2 surface antigens were de-multiplexed using Seurat. At the same time, cell clusters were identified based on gene expression data (GEX) from the integrated dataset, following a standard *Seurat* workflow. Unsupervised clustering revealed 14 clusters of cells, which included Tregs, T effectors, B cells, and nonlymphoid cells such as macrophages, dendritic cells, and neutrophils (data not shown). The analyses included in these studies constitute unsupervised clustering of lymphocytes.

TCR sequencing analysis

TCR data were processed and combined using the R library scRepertoire[35] following the standard workflow, and the resulting data were imported into the Seurat single-cell dataset as metadata. Various plots were generated using plotting functions from *Seurat*, *scRepertoire*, and R library, *ggplot2* (https://ggplot2-book.org/).

Statistical analysis

Statistical analyses (excluding sequencing data) were performed with GraphPad Prism version 10 (GraphPad Software). A P value of 0.05 or lower was accepted as significant. Normality was assessed using the Shapiro-Wilk test. Data is reported as the mean ± SEM.

Materials for all experimental techniques described are available in Table S1.

Results

CNS1 deletion causes exacerbated ALI in response to influenza infection

To understand the roles of peripherally induced Tregs arising via CNS1 in the recovery from ALI, we treated CNS1 knockout (ΔCNS1) and C57BL/6J (WT) mice with a mouse-adapted strain of H1N1 influenza, PR8, at a dose that induced roughly 40% mortality (or meeting of humane endpoint) in WT mice (ED40).[30] ΔCNS1 mice exhibit poorer survival from PR8 when compared with WT mice, and most mortality occurs days 9 to 12 post-PR8 (Fig. S1A). Weight loss following influenza is also more severe in ΔCNS1 mice, and the percentage difference from initial weight diverges from that of WT mice 11 d after infection (Fig. S1B, C). Blood oxygen saturation in ΔCNS1 mice is also significantly lower on days when weight loss and mortality diverge from WT mice (Fig. S1D). Although ΔCNS1 mice are more hypoxic and have higher rates of mortality or meeting humane endpoint (>30% weight loss from initial weight prior to infection) earlier or more often than WT mice on days of peak injury, ΔCNS1 mice do not experience differences in elevated markers of liver (alanine transaminase, aspartate transaminase) or kidney (creatinine) injury at this time point compared with WT (Fig. S1E–G), suggesting that acute lung injury leading to hypoxic respiratory failure is the cause of mortality or injury endpoint parameters.

To decrease the number of mice meeting humane endpoint so that we could better study disease pathology and recovery in ΔCNS1 mice, we used a lower dose of PR8 to induce ALI. This dose (ED20) resulted in more modest differences in mortality and weight loss in ΔCNS1 mice, and no overall histological differences were observed among surviving mice at day 16 post-infection (Fig. 1A–C). We observed elevated total lung cells and total cells/mL in the BAL fluid of ΔCNS1 mice collected at day 10 post-PR8 (Fig. 1D, E). However, these changes are not accompanied by elevated vascular leakage as measured by BAL total protein (Fig. 1F). Extended immune kinetics in ΔCNS1 and WT mice at steady state (naïve) and 3 time points after PR8-induced ALI are depicted in Fig. S2. When considering immune responses in the BAL compartment induced by the lower PR8 dose, we find elevated neutrophils, Ly6C$^+$ monocyte-derived macrophages, inflammatory macrophages, CD4$^+$, and CD8$^+$ lymphocytes in the BAL of ΔCNS1 mice at day 10 post-PR8 (Fig. 1G; Fig. S2C). Gating techniques for cells of the lymphoid and myeloid lineages are depicted in Figs. S3 and S4, respectively. Elevated cytokines in the BAL fluid supernatants were also observed at 10 d post-PR8, including IL-6, Eotaxin, G-CSF, KC, MCP-1, and RANTES, many of which have roles in recruiting the immune cells we observed to be elevated in the BAL at this time point (G-CSF: monocytes/macrophages; KC: neutrophils; MCP-1: monocytes/macrophages; RANTES: lymphocytes) (Table S2).[36]

Under naïve conditions, ΔCNS1 mice have a greater number of Ly6C$^-$ monocyte-derived macrophages and CD3$^+$, CD4$^+$, and CD19$^+$ lymphocytes in digested lung single-cell suspensions, suggesting a baseline difference in the lung microenvironment compared with WT (Fig. S2A). Additionally, at day 4 post-PR8, a time point of peak viral protein levels in epithelial cells (Fig. S5 and S6), we observed greater numbers of inflammatory macrophages and CD3$^+$ lymphocytes in the lungs of ΔCNS1 mice (Fig. S2B). There is also evidence of delayed resolution of the immune response in the lung compartment. First, we observe elevated T cell activation phenotypes in ΔCNS1 mice, including increased incidence of CD44$^+$CD62L$^-$ CD4$^+$ and CD8$^+$ T cells (Fig. 1H) and CD69$^+$ CD4$^+$ and CD8$^+$ T cells (Fig. 1I) 15 d post-PR8 in ΔCNS1 mice, a time point of early recovery in this ALI model (Fig. 1B). We also observed delayed resolution in cytokine production in ΔCNS1 mice, documented by increased geometric mean fluorescence intensity (MFI) of TNF-α in effector ΔCNS1 CD4$^+$ and CD8$^+$ T cells, as well as an increase in total TNF-α$^+$ CD4$^+$ T cells 15 d post-PR8 (Fig. 1J). Overall, even in ΔCNS1 mice that do not succumb to severe ALI, T cell activation is more significant compared with WT mice.

When considering tissue remodeling following injury, we found that ΔCNS1 mice have fewer total epithelial cells (CD326$^+$) during early recovery (Fig. 1K), indicating that ΔCNS1 Tregs are unable to perform tissue repair functions described previously in ALI,[16,17] or that the tissue damage caused during peak inflammation is greater, or epithelial repair is delayed in ΔCNS1 mice. This phenotype is not accompanied by increased infection of epithelial cells, as measured by PR8 nucleoprotein (NP) positivity in type II alveolar epithelial cells or total CD326$^+$ lung cells, detected by flow cytometry (Fig. S6A, B). This suggests that the loss of CNS1 does not affect susceptibility to infection or viral clearance at the time points studied. We also find that CNS1 loss does not affect AT2 cell proliferation as measured by Ki-67 positivity (Fig S6C). In fact, we observe AT2 proliferation to be higher in CNS1 mice at day 15 post-PR8, which could indicate a survival bias, delayed induction in AT2 proliferation, or greater AT2 proliferation due to a greater degree of injury. Together, these results indicate that immune resolution is delayed and that lung epithelial recovery is impaired in ΔCNS1 mice following ALI.

CNS1 deletion alters lung Treg phenotypes and CD4$^+$ T cell skewing

Tregs in ΔCNS1 mice do not increase in number to the same degree during early recovery from influenza as WT Tregs (Fig. 2A), and at all stages of ALI Tregs make up a smaller percentage of

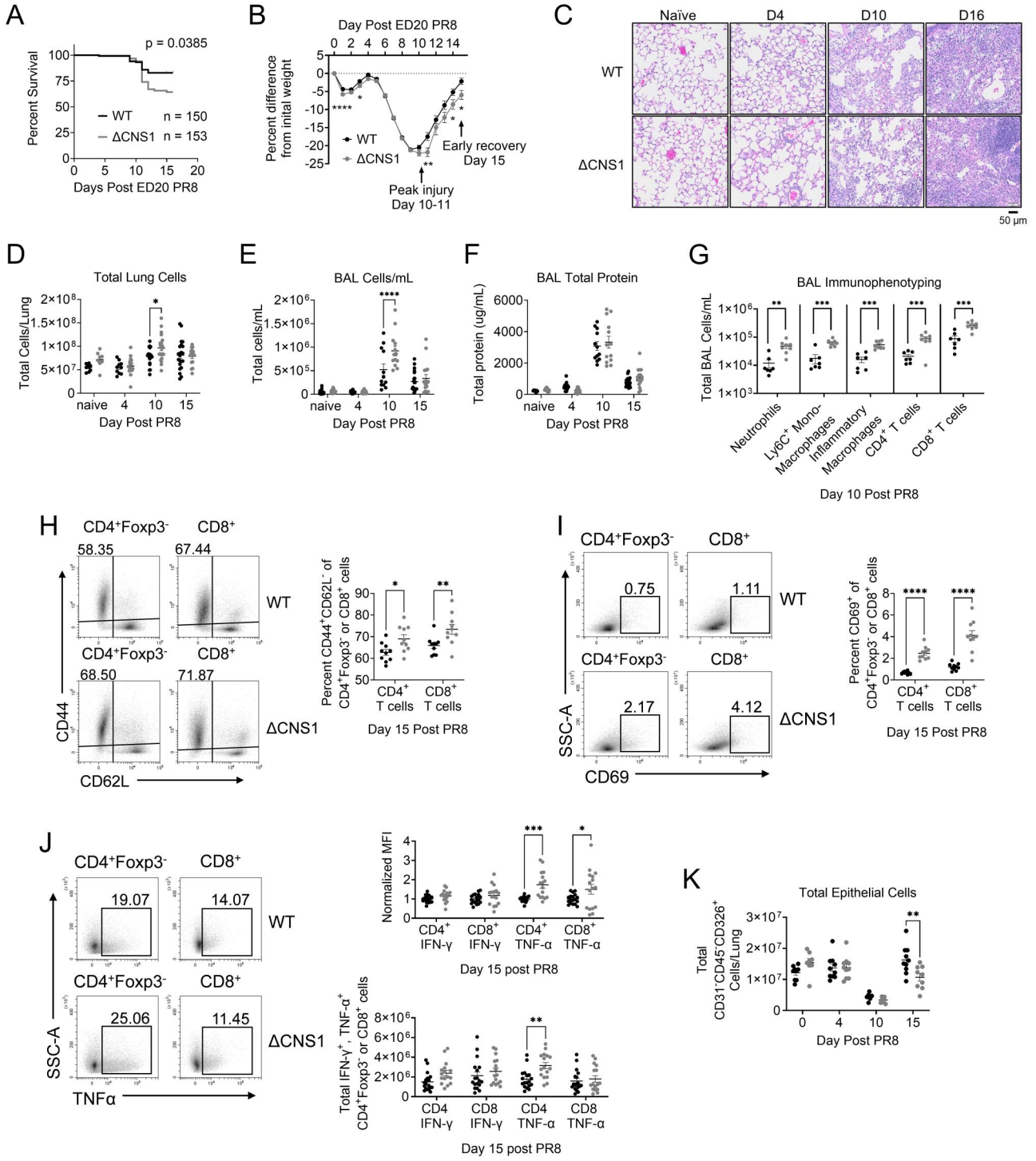

Figure 1 CNS1 deletion causes exacerbated ALI in response to ED20 influenza infection. (A) Survival following PR8 infection. Significance was determined via Kaplan-Meier survival analysis. (B) Weight loss kinetics following PR8 infection. (A, B) There were 150 to 153 male and female mice per strain, combination of 7 independent experiments. Significance was determined by multiple *t* tests. (C) Representative histological images from the lungs of WT and ΔCNS1 mice throughout PR8 infection. There were 6 to 10 male and female mice per strain, a combination of 2 independent experiments. (D) Total lung cells, (E) total cells/mL in the BAL, and (F) total protein concentration of BAL fluid in naïve, 4 d post-PR8, 10 d post-PR8, or 15 d post-PR8 in WT and ΔCNS1 mice. (G) Immune cell populations measured in the BAL fluid of WT and ΔCNS1 mice 10 d post-PR8. Significance determined by individual unpaired *t* tests. Percentage of $CD4^+$ and $CD8^+$ T cells that are (H) $CD44^+CD62L^-$ and (I) $CD69^+$ 15 d post-PR8. (J) Representative TNF-α flow plots (left), IFN-γ^+ and TNF-α^+ MFIs of $CD4^+$ and $CD8^+$ T cells (top right), and total IFN-γ^+ or TNF-α^+ $CD4^+$ and $CD8^+$ T cells (bottom right) 15 d post-PR8. Data collected with intravenous exclusion of $CD45^+$ cells. (K) Total $CD326^+$ epithelial cells in WT and ΔCNS1 mice throughout PR8. (D–I, K) There were 7 to 22 male and female mice per condition, a combination of 1 (days 4 and 10) and 2 (day 15) independent experiments per strain, or 1 independent experiment (naïve). (J) There were 16 to 18 male and female mice per strain, combination of 2 independent experiments. (G–I, K) Samples from genotypes processed separately on days 4, 10, and 15. Unless otherwise indicated, significance was determined by 2-way analysis of variance with Holm-Šídák's multiple comparisons test. $^*P < 0.05$, $^{**}P < 0.01$, $^{***}P < 0.001$, $^{****}P < 0.0001$. D, day; SSC-A, side scatter area.

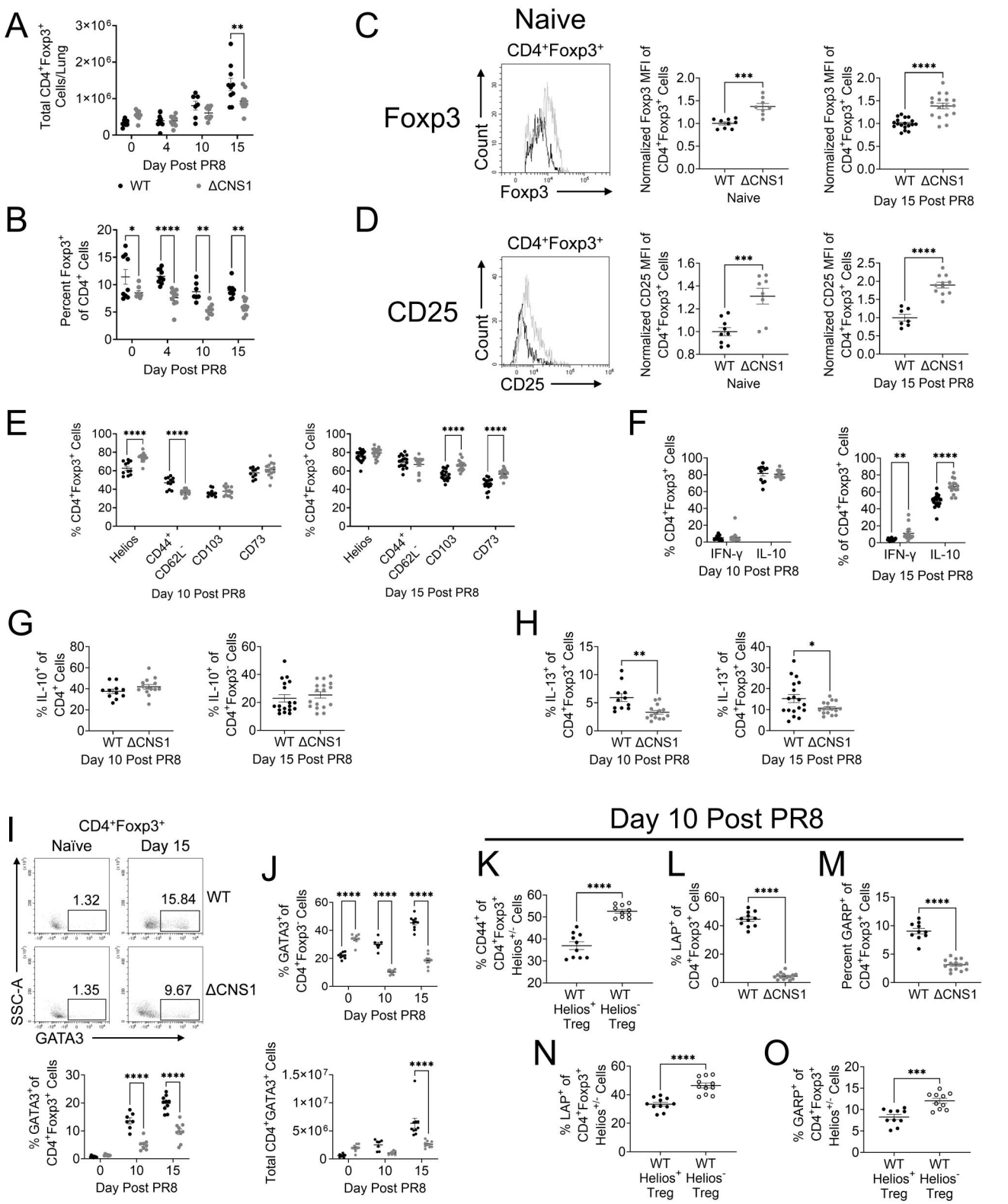

Figure 2 CNS1 deletion alters lung Treg phenotypes in ED20 influenza infection. (A) Total Tregs in the lungs of WT and ΔCNS1 mice throughout PR8 lung injury. (B) Tregs as a percentage of $CD4^+$ T cells in the lungs of WT and ΔCNS1 mice throughout lung injury. (C) Normalized Foxp3 MFI of $CD4^+Foxp3^+$ Tregs in WT and ΔCNS1 naïve (left histogram and dot plot) and 15 d post-PR8 (right) mice. (D) Normalized CD25 MFI of $CD4^+Foxp3^+$ Tregs in WT and ΔCNS1 naïve (left histogram and dot plot) and 15 d post-PR8 (right) mice. Day 15 data collected with intravenous CD45 exclusion of intravascular immune cells. MFI of each data point divided by the average of the WT data points. (E) Percent of Tregs that express each indicated functional surface marker or transcription factor in WT and ΔCNS1 mice at either day 10 or day 15 post-PR8. Helios data collected from stimulated cells, with other data collected from unstimulated cells from the same subjects. CD44 data collected with exclusion of $CD8^+$ cells. Data combined

Figure 2. Continued
from multiple panels and gating schemes. (F) Percent of Tregs that express each indicated secreted functional effector in WT and ΔCNS1 mice at either day 10 or day 15 post-PR8. (G) Percent of stimulated $CD4^+$ conventional T cells that express IL-10 at either day 10 or day 15 post-PR8. (H) Percent of stimulated Tregs in WT and ΔCNS1 mice that express IL-13 at either day 10 or day 15 post-PR8. (I) Percent of $GATA3^+$ Tregs in WT and ΔCNS1 mice throughout lung injury. Example flow plots and percentage of $GATA^+$ Tregs are provided. (J) Percent of $GATA3^+$ in $CD4^+$ $Foxp3^-$ cells and number of $CD4^+$ $Foxp3^-$ $GATA3^+$ in WT and ΔCNS1 mice throughout lung injury. (K) Percent $CD44^+$ of $Helios^+$ and $Helios^-$ WT Tregs at day 10 post-PR8. (L) Percent LAP^+ Tregs in WT and ΔCNS1 mice at day 10 post-PR8. (M) Percent $GARP^+$ Tregs in WT and ΔCNS1 mice at day 10 post-PR8. (N) Percent LAP^+ of $Helios^+$ and $Helios^-$ WT Tregs at day 10 post-PR8. (O) Percent $GARP^+$ of $Helios^+$ and $Helios^-$ WT Tregs. Day 15 data in E-H were collected with intravenous exclusion of $CD45^+$ cells. (A–C) Day 15; (I, J) n = 7–10 per strain, male and female mice, a combination of 1 (days 4 and 10) or 2 (day 15) independent experiments per strain, or 1 independent experiment (naïve); (E–H, K–O) n = 11–18 per strain, combination of 1 (day 10) or 2 (day 15) independent experiments; (C) day 10, n = 8 or 9 mice per strain, 1 independent experiment. (A, B) Days 4, 10, and 15; (C) day 15, samples from genotypes processed separately. Significance was determined by unpaired Student *t* test (C, D, G, H, K, L, M), Student paired *t* test (K, N, O), or 2-way analysis of variance with Holm-Šídák's multiple comparisons test (A, B, E, F, I, J). $^*P < 0.05$, $^{**}P < 0.01$, $^{***}P < 0.001$, $^{****}P < 0.0001$.

the $CD4^+$ T cell compartment in ΔCNS1 mice (Fig. 2B). At the naïve state and 15 d post-PR8, ΔCNS1 Tregs express higher levels of Foxp3 (Fig. 2C), a marker of Treg stability,[37] and CD25 (Fig. 2D), a marker of Treg suppressive function.[38] Expression of Treg-associated surface proteins and transcription factors measured at 10 or 15 d post-PR8 (Fig. 2E) showed that ΔCNS1 Tregs exhibited a higher percentage of cells expressing Helios—a disputed marker of tTregs[39–41][mdash]at day 10, but not at day 15 post-PR8. Expression of the activation marker CD44 was decreased on ΔCNS1 Tregs 10 d (but not 15 d) post-PR8. Expression of CD103, a tissue retention marker,[16] was increased on ΔCNS1 Tregs 15 d (but not 10 d) post-PR8. Expression of CD73, which allows Tregs to generate adenosine, contributing to an immunosuppressive environment,[42] was also increased on ΔCNS1 Tregs 15 d (but not 10 d) post-PR8. Across Treg intracellular effector molecules, ΔCNS1 Tregs exhibit elevated percent positivity of IFN-γ (Th1-like Treg marker that can either drive or suppress Th1 responses)[43] and IL-10 (an immunosuppressive cytokine)[44] at the early recovery time point of 15 d post-PR8 but not during peak injury at 10 d post-PR8 (Fig. 2F).

Previous studies concerning CNS1 in Tregs reported an increased incidence of IL-10–producing $CD4^+Foxp3^-$ T cells (Tr1 cells) in peripheral lymph nodes of ΔCNS1 mice[25]; however, we did not find a greater percentage of Tr1 cells among $CD4^+$ cells in the lungs of ΔCNS1 mice at 10 or 15 d post-PR8 (Fig. 2G). Lung Tregs from ΔCNS1 mice also exhibit decreased Th2 skewing during PR8 infection, documented by fewer $IL\text{-}13^+$ Tregs, which have previously been shown to facilitate ALI recovery (Fig. 2H).[8,10] Previous reports have shown that at steady state, ΔCNS1 mice exhibit elevated T helper 2 (Th2) cells in peripheral lymphoid tissue.[26] We show similar results. However, this Th2 skewing does not persist following PR8 treatment; instead, ΔCNS1 mice display decreased Th2 and Th2-like Treg skewing throughout ALI (measured by GATA3 expression) (Fig. 2I, J). Differences in Th2 skewing are less pronounced when considering total $GATA3^+CD4^+$ cells, potentially due to the large number of total $CD4^+$ cells (Fig. 2J, bottom). These results suggest that CNS1 may influence the effector $CD4^+$ T cell response either directly, by influencing T cell transcriptional programs following injury, or indirectly, through aberrant Treg interactions/altered immunosuppressive environment. Overall, these studies provide evidence that CNS1 plays a crucial role in establishing Treg phenotypes and influencing the Treg response to PR8.

A time point of interest for understanding the role of CNS1 in ALI was day 10 post-PR8, as this is when mortality begins to diverge between ΔCNS1 and WT mice (Fig. 1A). At day 10, lung ΔCNS1 Tregs exhibit decreased CD44 positivity and elevated Helios positivity (Fig. 2E). When considering WT $Helios^{+/-}$ Tregs, we observe that $Helios^-$ Tregs are enriched to be $CD44^+$ (Fig. 2K). Previous studies have identified $Helios^-$ Tregs as potential pTregs,[39,45] so elevated CD44 positivity in the $Helios^-$ subset could be indicative of recent effector T cell identity. When exploring other functional markers whose expression is impaired in ΔCNS1 Tregs, we observe that markers related to TGB-β mediated Treg activity (latency-associated peptide [LAP], glycoprotein A repetitions predominant [GARP]) were also decreased in CNS1 Tregs (Fig. 2L, M), while also exhibiting elevated expression in the WT $Helios^-$ Treg subset when compared with the WT $Helios^+$ Treg subset (Fig. 2N, O). These results indicate that the $Helios^-$ subset in WT mice is distinct from the $Helios^+$ subset in WT mice. While some studies of the transcription factor Helios suggest that it is a marker of thymic Tregs,[39,46] these results are disputed.[40,41] Likely, $Helios^+$ Tregs represent a stable population of Tregs, as Helios functions to maintain Treg identity and suppressive function,[47–49] although some have found Helios expression to be associated with, but not a determinant of, Treg stability.[50] While we do not show that Helios is a faithful marker of tTregs, our results show that $Helios^-$ Tregs are especially important for TGF-β–driven regulatory functions and suggest that this $Helios^-$ Treg subset plays a key role in resolution after ALI, which is of importance to this study, as the $Helios^-$ Treg response is diminished in ΔCNS1 mice.

B cell dynamics and germinal center formation in the absence of CNS1

Previous reports have found that the binding of transcription factors to CNS1 in the *Foxp3* locus directs the formation of T follicular regulatory (Tfr) cells.[51] Similarly, low-level Foxp3 expression in T follicular helper (Tfh) cells directs germinal center (GC) dynamics.[52] At baseline, ΔCNS1 mice exhibit elevated lung B cells (Fig. S2A). However, during injury, B cells in ΔCNS1 mice fail to increase in number to the same extent as in WT mice (Fig. S2D). Previous reports have found that ΔCNS1 mice have elevated GC B cells at peripheral sites.[26] When characterizing GCs that form in the lung following injury, we find similar numbers of $B220^+GL\text{-}7^+MHCII^{hi}$ GC B cells in WT and ΔCNS1 mice across injury time points (Fig. 3A). Interestingly, GC B cells decrease following injury, possibly due to B cell maturation into plasma cells during infection (Fig. 3A).[53] Notably, ΔCNS1 lung, but not spleen

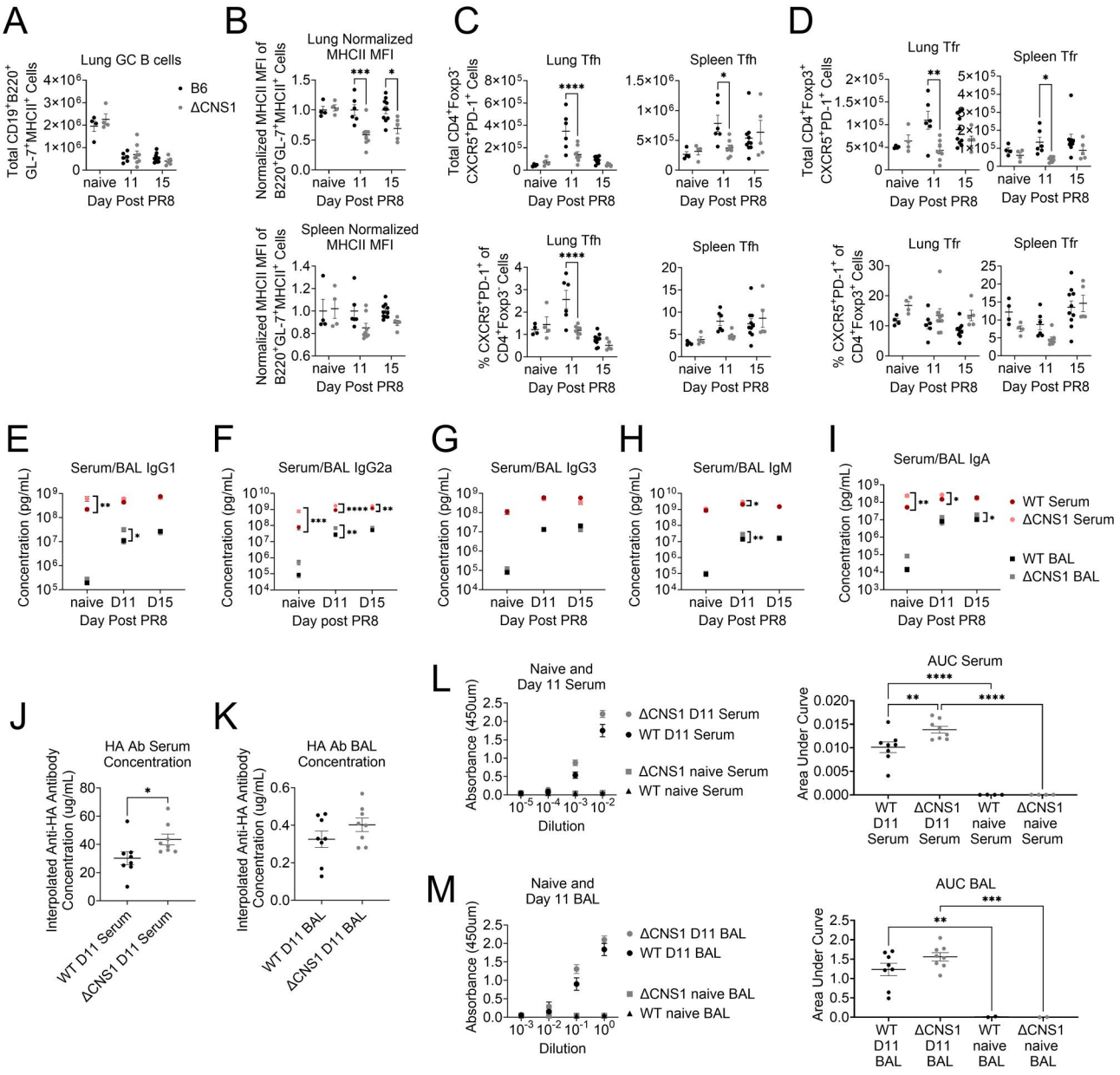

Figure 3 Effects of CNS1 deletion on antibody responses, B cell dynamics, and GC formation following ED40 PR8. (A) Total lung GC B cells at steady state and 2 time points of PR8-induced lung injury. (B) MHCII MFI of GC B cells in the lung (top) and spleen (bottom). (C) Lung (left) and spleen (right) Tfh cells expressed as total numbers (top) and as a percentage of total $CD4^+Foxp3^-$ cells (bottom) at steady state and 2 time points of PR8-induced lung injury. (D) Lung (left) and spleen (right) Tfr cells expressed as total numbers (top) and as a percentage of total $CD4^+Foxp3^+$ cells (bottom) at steady state and 2 time points of PR8-induced lung injury. (E–I) Serum and BAL IgG1 (E), IgG2a (F), IgG3 (G), IgM (H), and IgA (I) in naïve, day 11, and day 15 post-PR8. Significance was determined via 2-way analysis of variance with Holm-Šídák's multiple comparisons test separately for serum and BAL. (J–K) Interpolated serum (J) or BAL (K) concentrations of HA-specific IgG. Significance determined by an unpaired Student *t* test. (L, M) Dilution curves of HA-specific IgG from either serum (L) or BAL (M) from naive or day 11 post-PR8 time points (left) with area under the curve (right). Significance was determined by 1-way analysis of variance with Holm-Šídák's multiple comparisons test. n = 4–10 per strain, combination of 1 independent experiment (A–D); n = 2–8 per condition, combination of 1 to 2 independent experiments (E); n = 6–20 per strain, male and female mice, 1 independent experiment (F–J); n = 2–8 per condition, male and female mice, combination of 2 independent experiments (K–N). Unless otherwise stated, significance was determined by 2-way analysis of variance with Holm-Šídák's multiple comparisons test. $^*P < 0.05$, $^{**}P < 0.01$, $^{***}P < 0.001$, $^{****}P < 0.0001$.

GC B cells, exhibit decreased MHCII expression as measured by MFI 11 and 15 d post-PR8 (Fig. 3B), indicating that these GC B cells may be less functional or engage less with Tfh cells,[53] as we observe fewer Tfh cells in ΔCNS1 mice at day 11 post-PR8 (Fig. 3C). CNS1 loss does not affect the potential of Tregs to adopt the Tfr fate (Fig. 3D, bottom); however, we report fewer total Tfr cells at peak injury in the lung and spleen (Fig. 3D, top), potentially due to decreased Tfh and/or B cell engagement.

Gating schemes for Tfh, Tfr, and GC B cells are depicted in Figure S7. These results further suggest that either CNS1 activity in $CD4^+$ T cells facilitates T cell polarization in response to infection, or CNS1 activity in Tregs promotes the development of Tfh cells that support GC development and maturation in ALI.

CNS1 deletion alters antibody production at steady state and during ALI but not the response to the PR8 antigen, HA

Previous reports have found that ΔCNS1 mice have exhibited antibody reactivity to antigens associated with the mucosa.[26] Here, we report that serum and BAL supernatant samples from ΔCNS1 mice exhibit aberrant Ig skewing at baseline and throughout the injury process. We observe elevated baseline IgG1, IgG2a, and IgA serum production in ΔCNS1 mice, and elevated serum and/or BAL IgG1, IgG2a, IgA, and IgM in ΔCNS1 mice at peak and/or resolving injury (Fig. 3E–I). In ΔCNS1 mice, antibody responses were broadly elevated compared with WT control mice in both serum and BAL. IgM levels were elevated at peak injury in both compartments, consistent with an amplified early-phase antibody response. Serum IgG2a concentrations were elevated across all studied time points, indicating enhanced baseline and ALI-induced antibody production. IgA levels were also higher, particularly during early recovery in BAL and at baseline and peak injury in serum, suggesting increased mucosal-associated antibody responses. In contrast, IgG3 levels remained unchanged, indicating selective enhancement of antibody subclasses in ΔCNS1 mice during lung injury and repair.

When detecting the existence and development of autoantibodies in ΔCNS1 mice via autoantigen microarray, we, like others[26] observe elevated serum autoantibodies in ΔCNS1 mice at baseline (Fig. S8, Table S3). At peak injury and early recovery (days 11 and 15), ΔCNS1 mice also exhibit elevated autoantibodies when compared with WT mice; however, the number of elevated autoantibodies in ΔCNS1 mice at these time points is not as significant as in naïve mice (Fig. S8, Table S3).

To further understand the PR8-specific antibody response, we performed PR8 HA-directed ELISA analyses of serum from WT and ΔCNS1 mice. We found that ΔCNS1 mice exhibited a higher concentration of HA-specific IgG in the serum but unchanged HA-specific IgG in the BAL when compared with WT mice (Fig. 3J–M). Overall, we report differential antibody production and skewing in ΔCNS1 mice; however, the serologic response to a PR8 antigen in ΔCNS1 mice does not appear impaired when compared with WT mice.

CNS1-deficient Tregs have an impaired ability to develop TCR reactivity to a common PR8 antigen

Early literature on ΔCNS1 mice found that Treg development of TCRs specific for non–self-antigens is impaired.[25] Later studies have clarified that Treg induction in ΔCNS1 mice may still occur,[54] although this process is delayed.[21] In models of infection, recent reports have established that self-reactive Tregs repress overactive inflammation driven by conventional $CD4^+$ T cells to promote a productive response to infection rather than autoimmunity.[55] However, the process of antigen-specific Treg development that is dependent upon CNS1 in ALI is currently undescribed. Thus, we assessed the role of CNS1 in the development of Treg reactivity to the common influenza antigen, NP, which has previously been reported to develop during ALI.[5] Notably, CNS1 deletion does not prevent the development of NP tetramer–reactive $CD8^+$ (Fig. 4A) or $CD4^+$ (Fig. 4B) effector cells at either day 10 or day 15 post-PR8. Most of these cells are restricted to the lung and are not detected in the spleen (Fig. 4A, B). We also found CNS1-dependent functions in supporting the development of NP-reactive Tregs (Fig. 4C–H). NP-reactive Tregs are primarily restricted to the lung in WT mice, and that the development of NP-reactive lung Tregs in ΔCNS1 mice was significantly lower at both day 10 and day 15 following PR8 (Fig. 4C, F).

While NP tetramer–reactive Tregs make up a small fraction of total Tregs in WT mice, we nevertheless wanted to understand how tetramer-reactive Tregs differ from the total Treg pool. First, Foxp3 expression is lower in tetramer-reactive Tregs than in the total Treg pool (Fig. 4D, G). Second, most tetramer-reactive Tregs are $Helios^-$. Third, tetramer-reactive Tregs are also more likely than the total Treg pool to express Ki-67, a marker of proliferation; CCR4, a marker of Treg suppressive function (only 15 d post-PR8); and CXCR3, a Th1 chemokine receptor, and more likely to express CD103 (a tissue-resident marker) at day 10 following PR8 and less likely to express CD103 at day 15 following PR8 (Fig. 4E, H).

To further understand pTreg development in WT mice, we assessed for Foxp3 expression in adoptively transferred $CD45.2^+$ $CD4^+$ $Foxp3^-$ cells from transferred splenocytes obtained from naïve *Foxp3*^{DTR} mice, which allow for transferred Tregs to be depleted with diphtheria toxin administration after transfer (Fig. 4I). After diphtheria toxin administration and PR8-induced lung injury, we examined for Foxp3 expression specifically in transferred $CD45.2^+$ $CD4^+$ cells 15 d post-PR8 in the recipient ($CD45.1^+$ $CD45.2^+$) mice (Fig. 4I). We found that the donor population of $CD4^+$ cells does induce Foxp3 expression, albeit at a lower rate compared with Foxp3 expression in the recipient $CD4^+$ T cell population (Fig. 4J). Similar to our NP tetramer results, we observe that the induced donor pTreg population displays a significantly lower level of Foxp3 expression when compared with the recipient Treg pool after PR8 injury (Fig. 4K).

To understand whether transfer of WT $CD4^+$ T cells provide benefit to ΔCNS1 mice undergoing PR8-induced ALI, we adoptively transferred $CD4^+CD25^-$ T cells purified from the lungs and spleens of PR8-treated *Foxp3*^{DTR} or ΔCNS1 mice (Fig. 4L, left). Recipient ΔCNS1 mice from both groups were subsequently treated with PR8 followed by diphtheria toxin 1 day after infection. We observed that adoptive transfer with $CD4^+$ ($CD25^+$ bead-depleted) T cells from donor *Foxp3*^{DTR} mice resulted in significantly improved survival when compared with $CD4^+$ ($CD25^+$ bead-depleted) T cells from ΔCNS1 donor mice (Fig. 4L, right).

In summary, these studies show that CNS1 deletion impairs the development of antigen-specific (NP-reactive) Tregs in the lung following influenza-induced injury, without inhibiting effector $CD4^+$ or $CD8^+$ responses. Tetramer-reactive Tregs exhibit lower Foxp3 expression, are largely $Helios^-$, and display markers consistent with proliferative, Th1-skewed, and tissue-resident phenotypes, suggesting that they may arise from peripherally induced Tregs adapted to inflamed lung environments.

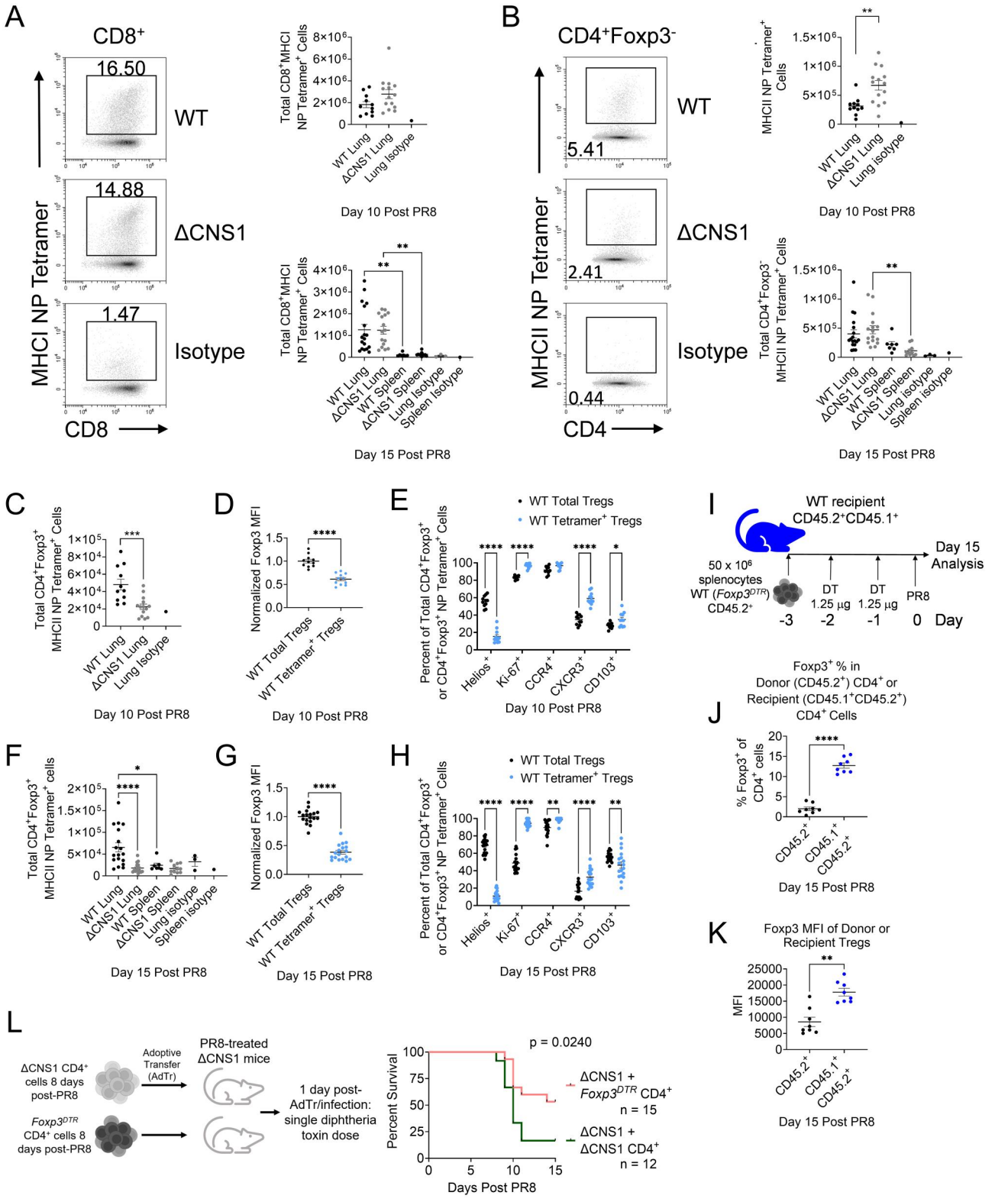

Figure 4 CNS1-deficient Tregs have impaired ability to develop TCR reactivity to a common PR8 antigen following ED20 PR8. (A) Representative flow plots of NP tetramer–reactive $CD8^+$ T cells, with percent positivity indicated (left). Total NP tetramer–reactive $CD8^+$ T cells (right). Data presented from 10 (top) or 15 (bottom) days post-PR8. (B) Representative flow plots of NP tetramer–reactive $CD4^+Foxp3^-$ T cells, with percent positivity indicated (left). Total NP tetramer–reactive $CD4^+Foxp3^-$ T cells (right). Data presented from 10 (top) and 15 (bottom) days post-PR8. (C, F) Total NP tetramer–reactive $CD4^+Foxp3^+$ Tregs. Data presented from 10 (C) and 15 (F) days post-PR8. (D, G) Foxp3 MFI of WT total Tregs and WT NP tetramer–reactive Tregs, normalized to the average of all the Foxp3 MFIs of the WT total Tregs 10 (D) or 15 (G) d post-PR8. Significance was determined via a paired Student *t* test (D, G). (E, H) Percent effector marker positivity of total WT Tregs and WT NP tetramer–reactive Tregs 10 (E) or 15 (H) d post-PR8.

Figure 4. Continued
(A–H) Data collected on day 15 included CD45 intravenous exclusion. n = 11–18 per strain, combination of 1 (day 10) or 2 (day 15) independent experiments; male and female mice. (I) Experimental schematic for adoptive transfer experiment (J, K) in which splenocytes from donor mice (*Foxp3*^{DTR} mice; CD45.2^{+})[3] were administered to congenic, WT recipients that were CD45.1^{+}CD45.2^{+}. Adoptively transferred Treg were depleted 24 and 48 h post–adoptive transfer with diphtheria toxin (DT) before infection with PR8 H1N1 at 72 h post–adoptive transfer. (I–K) The stock PR8 used for the ED40 treatments was diluted further to approximately 1.875 × 10^{4} EID/mL in PBS to lessen mortality. (J) Tregs from either donor (CD45.2^{+}; induced post-DT) or recipient (CD45.1^{+}CD45.2^{+}) as a percentage of CD4^{+} T cells in the lungs at day 15 post-PR8. (K) Foxp3 MFI of CD4^{+}Foxp3^{+} Tregs from either donor (CD45.2^{+}) or recipient (CD45.1^{+}CD45.2^{+}) at 15 day post-PR8. n = 8 from 1 experiment. (L) Adoptive CD4^{+}CD25^{-} T cell transfer of *Foxp3*^{DTR} and CNS1 cells into CNS1 mice (left), mortality from influenza infection (ED40) in recipient mice (right). n = 7 or 8 mice (male and female) from 2 combined experiments; significance determined via Kaplan-Meier survival analysis. Unless otherwise stated, significance determined via 1-way analysis of variance with Holm-Šídák's multiple comparisons test (A [day 15], B [day 15], F), 2-way analysis of variance with Holm-Šídák's multiple comparisons test (E, H), unpaired *t* test (A [day 10], B [day 10], C, J–K), or paired Student *t* test (D, G). *$P < 0.05$, **$P < 0.01$, ***$P < 0.001$, ****$P < 0.0001$.

CNS1 deletion affects several Treg phenotypes in a cell-intrinsic manner

Increased mortality in ΔCNS1 mice (Fig. 1A; Fig. S1A), accompanied by increased expression of Treg markers associated with enhanced function (Fig. 2C–F), raised the possibility that Treg phenotypes in ΔCNS1 mice arose as a compensatory mechanism or due to missing or aberrant signals in the lung microenvironment. To understand potential compensatory events in ΔCNS1 mice and to decouple lung development from ALI challenge, we performed mixed bone marrow chimera experiments. We delivered a mixture of splenocytes and bone marrow from WT and ΔCNS1 mice to irradiated CD45.1^{+} CD45.2^{+} WT recipient mice (sexes matched between recipient and donor) 1 d following recipient irradiation (Fig. 5A). After 8 wk of reconstitution, we detected both donor and recipient populations of Tregs in lungs and spleens (Fig. 5A, B). Overall, ΔCNS1 cells exhibit a trend toward a greater contribution of Tregs than adoptively transferred WT Tregs at 8 wk post-engraftment in steady-state (naïve) mice. However, these advantages did not persist following ALI. Following PR8-induced ALI, we observed that Tregs from all groups increased but that this increase was not statistically significant among ΔCNS1 Tregs at day 15 post-PR8 (Fig. 5B, top), potentially indicating that ΔCNS1 Tregs are worse-suited to the ALI response.

We also measured total and fractional CD4^{+} and CD8^{+} cell engraftment and expansion (Fig. 5C, D). Percent engraftment of ΔCNS1 CD4^{+} and CD8^{+} cells as a percentage of total CD4^{+} and CD8^{+} cells is elevated compared with WT engraftment, but effector T cell dynamics shift throughout ALI (Fig. 5C, D).

We report several Treg-intrinsic effects of CNS1 loss. These include elevated Treg Foxp3 expression (Fig. 5E), elevated Treg Helios positivity (Fig. 5F), elevated CD103 positivity (Fig. 5G), and elevated IFN-γ positivity at day 15 post-PR8 (Fig. 5H). We also observed that ΔCNS1 Tregs in chimeric mice exhibit decreased CD44 positivity (Fig. 5I), a phenotype also observed in ΔCNS1 mice only at day 10 post-PR8. We also report that several Treg phenotypes do not persist in chimeric ΔCNS1 Tregs, including LAP (Fig. 5J), GARP (Fig. 5K), and IL-10 positivity (Fig. 5L). Our results indicate that ΔCNS1 Tregs may receive cues from the chimeric microenvironment that they do not in nonchimeric experiments, resulting in several Treg phenotypes that do not persist in chimeric mice (e.g. GARP, LAP, IL-10 expression). Table S4 lists phenotypes observed in chimeric and nonchimeric mice and provides a summary of our conclusions regarding which Treg phenotypes are cell intrinsic.

Because splenic and bone marrow transplants may not fully recapitulate the phenotypes of lung-resident Tregs and CNS1's potential influences on the lung microenvironment, we also generated heterozygote ΔCNS1 × *Foxp3*^{DTR} and JAXboy × *Foxp3*^{DTR} mouse strains. Because Foxp3 is on the X chromosome and because random X inactivation occurs in females, the resulting heterozygosity in F1 female ΔCNS1 × *Foxp3*^{DTR} mice allowed ΔCNS1 Tregs to develop in the presence of WT Tregs. We then depleted WT *Foxp3*^{DTR} Tregs with diphtheria toxin treatment throughout PR8-induced ALI to isolate the effects of CNS1 loss in ALI (Fig. 5M). We found that CNS1 contributes to suppression of CD4^{+} T cell expression of Th1 cytokines IFN-γ (Fig. 5N) and TNF-α (Fig. 5O), and that whole-body ΔCNS1 mice seem to develop the ability to suppress Th1 cytokine expression in a compensatory manner.

CNS1 mediates Treg gene expression in ALI

To understand the cell-intrinsic contributions of CNS1 to Treg and CD4^{+} effector T cell transcriptomes, we subjected lung cells from bone marrow chimeric mice to Treg isolation via bead-based enrichment, followed by single-cell RNA sequencing, TCR sequencing (TCRseq), and CITE-seq (to identify cells based on their expression of CD45.1^{+} and/or CD45.2^{+}) at naïve conditions or at day 10 or 15 post-PR8 infection (Fig. 6A). Unsupervised clustering of lymphocytes revealed 14 distinct clusters (Fig. 6B). CITE-seq separated cell sources resulted in detection of CD45.2^{+} (WT) and CD45.1^{+} CD45.2^{+} (recipient) cells at the naïve time point; detection of CD45.2^{+}, CD45.1^{+} CD45.2^{+}, and CD45.1^{+} (ΔCNS1) cells at the day 10 post-PR8 time point; and detection of CD45.2^{+} and CD45.1^{+} cells at the day 15 post-PR8 time point (Fig. 6C; Fig. S9A). Donor and recipient contributions to each cluster at each time point are depicted in Figure S9A–D. *Foxp3* expression by cluster is depicted in Figure 6D. Table S5A depicts cell frequencies from each cell source at each time point.

Clusters 0, 1, 4, 5, and 7 represented different Treg clusters. Cluster 0 was driven by expression of T central memory–related genes (*Ccr7*, *Sell*, *Klf2*, *Bach2*, *Klf3*, *Lef1*, *Gimap6*).[56] Cluster 1 was driven by expression of genes associated with Treg suppressive function (*Foxp3*, *Ly6a*, *Tigit*, *Glrx*, *Ctla4*, *Ifngr1*, *Tnfrsf4*, *Ccr2*, *Gimap7*, *Ikzf2*).[57] Cluster 2 was driven by proliferation genes (*Lgals1*, *Pclaf*, *Stmn1*, *Birc5*, *Mki67*, *Cdca8*, *Cdk1*, *Ccna2*, *Cdca3*) 58—60 and includes CD4^{+} cells, CD8^{+} cells, and Tregs. Cluster 3 was driven by innate lymphoid-related genes (*Lmo4*, *Trdv4*, *Ramp1*, *Gata3*, *Rora*, *Ccr8*, *Id2*, *Il5*, *Il13*). Cluster 4 was driven by

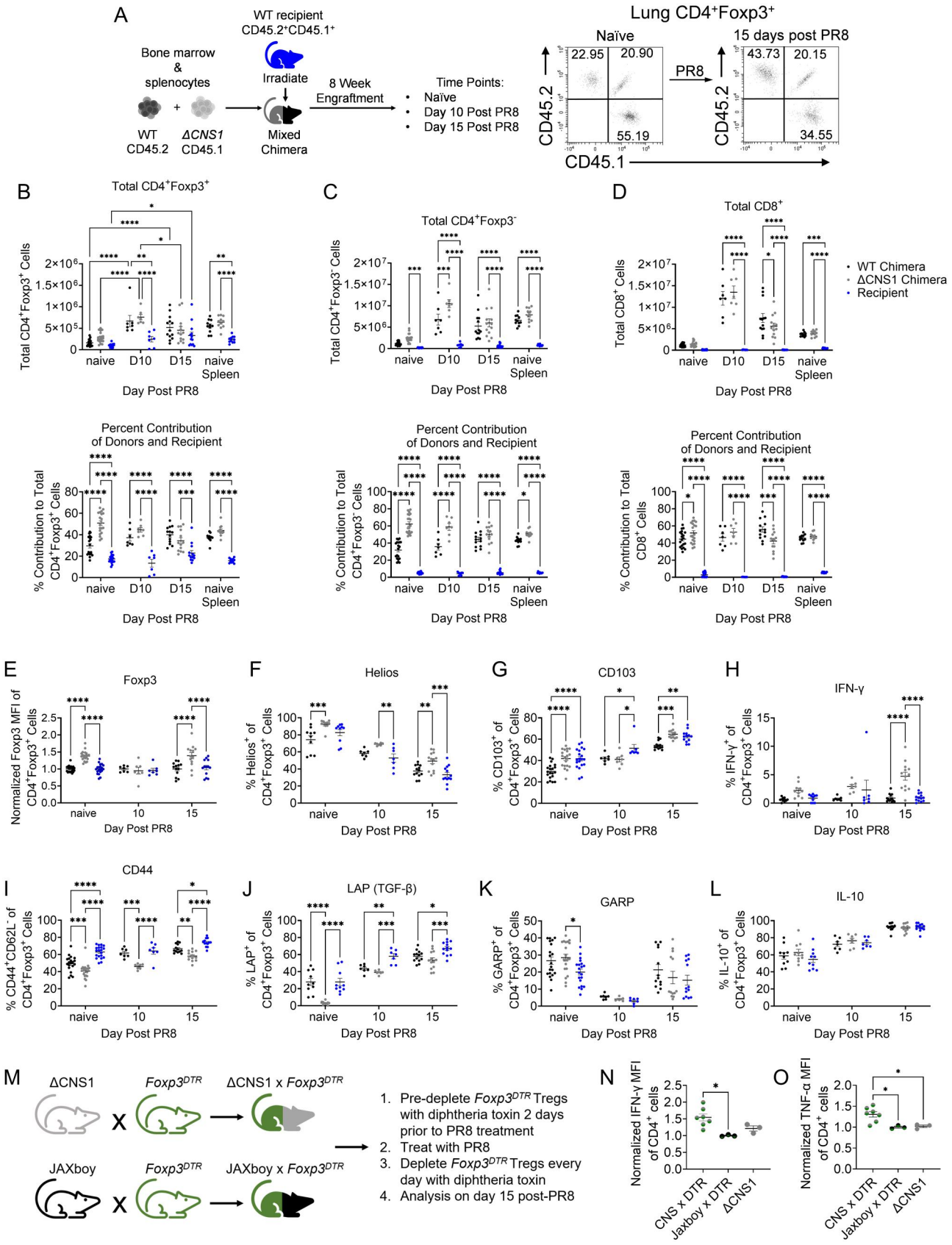

Figure 5 CNS1 deletion affects Treg phenotypes in a cell-intrinsic manner. (A) Experimental schematic for bone marrow chimera generation and analysis. A mixture of bone marrow and splenocytes from donor mice was administered to congenic, irradiated, WT recipients in a 2:1 ratio. Eight weeks following transplantation, naïve mice were studied to understand engraftment. Alternatively, mice were infected with PR8 and analyzed at

Figure 5. Continued
either 10 d (D10) or 15 d (D15) postinfection. (B) Engraftment (naïve) and expansion (D10, D15) analysis of total lung and spleen Tregs. (C) Engraftment (naïve) and expansion (D10, D15) analysis of total lung and spleen $CD4^+Foxp3^-$ cells. (D) Engraftment (naïve) and expansion (D10, D15) analysis of total lung and spleen $CD8^+$ cells. (E) Normalized Foxp3 MFI of Tregs. Each data point was divided by the WT MFI average at the same time point. Percentage of $Helios^+$ (F), $CD103^+$ (G), INF-γ^+ (H), $CD44^+$ (I), LAP^+ (J), $GARP^+$ (K), and IL-10^+ (L) Tregs. (M) Schematic of CNS1 × $Foxp3^{DTR}$ heterozygote experimental model). Normalized IFN-γ (N) and TNF-α (O) MFI of $CD4^+Foxp3^-$ T cells in heterozygote female F1 ΔCNS1 mice crossed to $Foxp3^{DTR}$ mice compared with control groups. (A–L) Data presented from 1 (D10) or 2 (naïve, D15) independent experiments. n = 20 (naïve), 7 (D10), and 13 (D15). (M, N) Data presented from 1 independent experiment, n = 3–7, female mice only. Significance was determined via 2-way analysis of variance with Holm-Šídák's multiple comparisons test (A–L), or 1-way analysis of variance with Holm-Šídák's multiple comparisons test. $^*P < 0.05$, $^{**}P < 0.01$, $^{***}P < 0.001$ $^{****}P < 0.0001$.

genes relating to Treg activation and migration into tissue (*Cd44*, *Maf*, *Icos*, *Capg*, *Tnfrsf4*, *Ccr4*, *Ccr6*, *S100a11*, *Hopx*, *Tigit*).[57,61–67] Cluster 5 included Tregs distinguished by the expression of mitochondrial-associated genes (*mt-Co1*, *mt-Atp8*, *Mbnl1*, *Ptrpc*, *Inpp4b*, *mt-Nd4l*, *Ets1*), leading us to conclude that cluster 5 Tregs are more likely to be apoptotic.[68] However, they still express Treg-associated genes (Fig. 6E). Cluster 6 represented cytotoxic CD8 T cells, which was distinguished by expression of *Nkg7*, *Ly6c2*, *Actb*, *Lgals3*, *Lgals1*, *Anxa2*, *Clf1*, *Gzmb*, *Pfn1*, *Ccl4*, *Klrd1*, *Gzma*, *Gzmk*, *Thy1*, *Ccl5*, and *Ifng*. Cluster 7 was distinguished by the elevated expression of genes related to migration,[69,70] cytokine signaling,[71] and virus response,[72,73] such as *Fau*, *Arhgap15*, *Klf2*, *Inpp4b*, and *Samhd1*, so we termed these cells "migratory Treg." Cluster 8 was mostly represented in the sample derived from day 10 post-PR8 and was driven by expression of *Birc5*, *Pclaf*, *Ccnb2*, *Cdca3*, *Mcm5m*, *Ccna2*, *Lgals3*, *Tbx21*, *Gzma*, *Gzmk*, *Mki67*, and *Cxcr3*, so we termed this cluster "early effector CD8."[74] Cluster 9 represented natural killer (NK) cells and exhibited enriched expression of *Fcer1g*, *Nrgn*, *Klrb1f*, *Ncr1*, *Xcl1*, *Clnk*, *Tyrobp*, *Car2*, and *Klrb1b*.[75] Cluster 10 included Th17 cells and included expression of Th17-related genes (*Il23r*, *Tmem176b*, *Tmem176a*, *Il1r1*, *Il17re*, *Ramp1*, *Il7r*, *Il18r1*, *Rorc*, *Cxcr6*, *Ccr6*, *Il17a*, *Rora*).[76] Cluster 11 represented NKT cells and included elevated expression of NKT-related genes (*Nkg7*, *Krt17*, *Stfa3*, *Klrd1*, *Xcl1*, *Tcf7*, *CD81b*, *Cxcr6*, *Ifng*, *Ly6c2*, *Ccl5*, *Cd8a*, *Cxcr3*).[77] Cluster 12 included γδ T cells[78] and exhibited upregulation of *Slc8a1*, *Tuba8*, *Alox5*, *Rgs18*, *Hes1*, *Lif*, *Trgc4*, *Trdv4*, *Il5*, *H2ac10*, *Nusap1*, *Pbk*, and *Kit*. Cluster 13 included gene expression patterns of B cells and also signatures of Treg fate (*Iglc3*, *Cd79a*, *CD24a*, *Blnk*, *Pou2af1*, *Iglc2*, *Mzb1*, *Iglc2*, *Cd19*).[56] A heatmap showing all clusters with cluster-defining genes is in Figure 6E. Table S5B lists differentially expressed genes (DEGs) driving each cluster.

Some of the defined clusters were biased towards specific time points and particular donor or recipient cells. Cluster 0 was predominantly present in the naïve sample, while clusters 1, 5, 6, 7, 8, and 10 were enriched in the day 10 post-PR8 sample. Cluster 4 was enriched in the day 15 post-PR8 sample, indicating that these Tregs may be important in facilitating early recovery (Fig. 6C).

Analysis of transcription factors associated with T cell fate reveals differential phenotypes over time, across clusters, and among donors (Fig. S10A, B). All Treg clusters express *Ikzf2* (Helios), including cluster 1. Additionally, we observe a decrease in the percentage of cluster 1 Treg expression of *Rora* in ΔCNS1 cells on days 10 and 15. *Gata3* expression also differed among donors, with greater expression observed in cluster 1 among WT than ΔCNS1 Tregs. Expression of *Bcl6* is low across all clusters, which is unsurprising, as Tfh cells and Tfr cells make up a small proportion of their parent populations (Fig. 3C, D). Expression of *Tbx21* was also low across all time points, potentially due to comparatively high expression in clusters containing $CD8^+$ T cells.

Cluster 7 at day 10 was a subset of interest, as day 10 post-PR8 (a time point of divergent ΔCNS1 mortality) was the only time point at which this subset was detected (Fig. 6C). Only 1 gene was differentially expressed at this time point between WT and ΔCNS1 cells: *Ifi208*, a member of a gene family induced in response to interferon signaling and involved in recognizing foreign DNA and activating the inflammasome through coordination with AIM2.[79] This DEG is downregulated in the ΔCNS1 cells in this cluster and in many other clusters.

Cluster 4 was enriched at day 15 post-PR8 (Fig. 6C); however, there were only 2 DEGs between WT and ΔCNS1 cells at this time point. Both *Camk2b*, calmodulin-dependent protein kinase family member beta chain (protein subunit beta), which is involved in the glutamatergic synapse, dendrite formation, neuronal morphology, and migration, apoptosis, autophagy, and myelination,[80] and *Ctla2a* (Treg effector molecule whose expression is increased with inducible Treg generation with TGF-β signaling)[81] are decreased in ΔCNS1 cells of this cluster.

When comparing gene expression between donor sources, we find that at day 10 *Foxp3* gene expression is elevated in the WT ($CD45.2^+$) cells compared with the ΔCNS1 ($CD45.1^+$) cells in cluster 1 (Fig. 6F). This suggests that CNS1-induced pTregs may fall into this cluster. Further analysis of gene expression differences between WT and ΔCNS1 transcriptomes in cluster 1 revealed that ΔCNS1 Tregs exhibit elevated Th1 and cytokine signaling signatures (decreased *Dusp1*, increased *IL6st*)[82,83] and naïve and early effector Treg/T effector cell signatures (*Sell*, *CD27*),[84,85] with decreased signatures associated with Th17 (and tissue Treg) fate/function (*Rora*)[86]; decreased *Il1rl1* (ST-2) expression (ST-2 was previously shown to protect the lung from severe influenza-induced ALI)[5]; decreased expression of regulators of G protein signaling *Rgs1* and *Rgs2*; decreased expression of Treg differentiation-related genes (*Ctla2a*, *Ctla2b*)[81]; TGF-β–dependent growth signatures (*Emb*)[87]; decreased expression of *Myadm*, a gene associated with tissue-residency[88]; and decreased expression of *Gmfg*, which is associated with cell migration and adhesion.[89] ΔCNS1 cells in cluster 1 also report elevated expression of *Ikzf3*, a member of the *Ikaros* gene family (also in this family is *Ikzf2*, which encodes Helios).[90] Overall, these results suggest differences in Treg polarization, with elevated *Foxp3* transcription and increased migration,

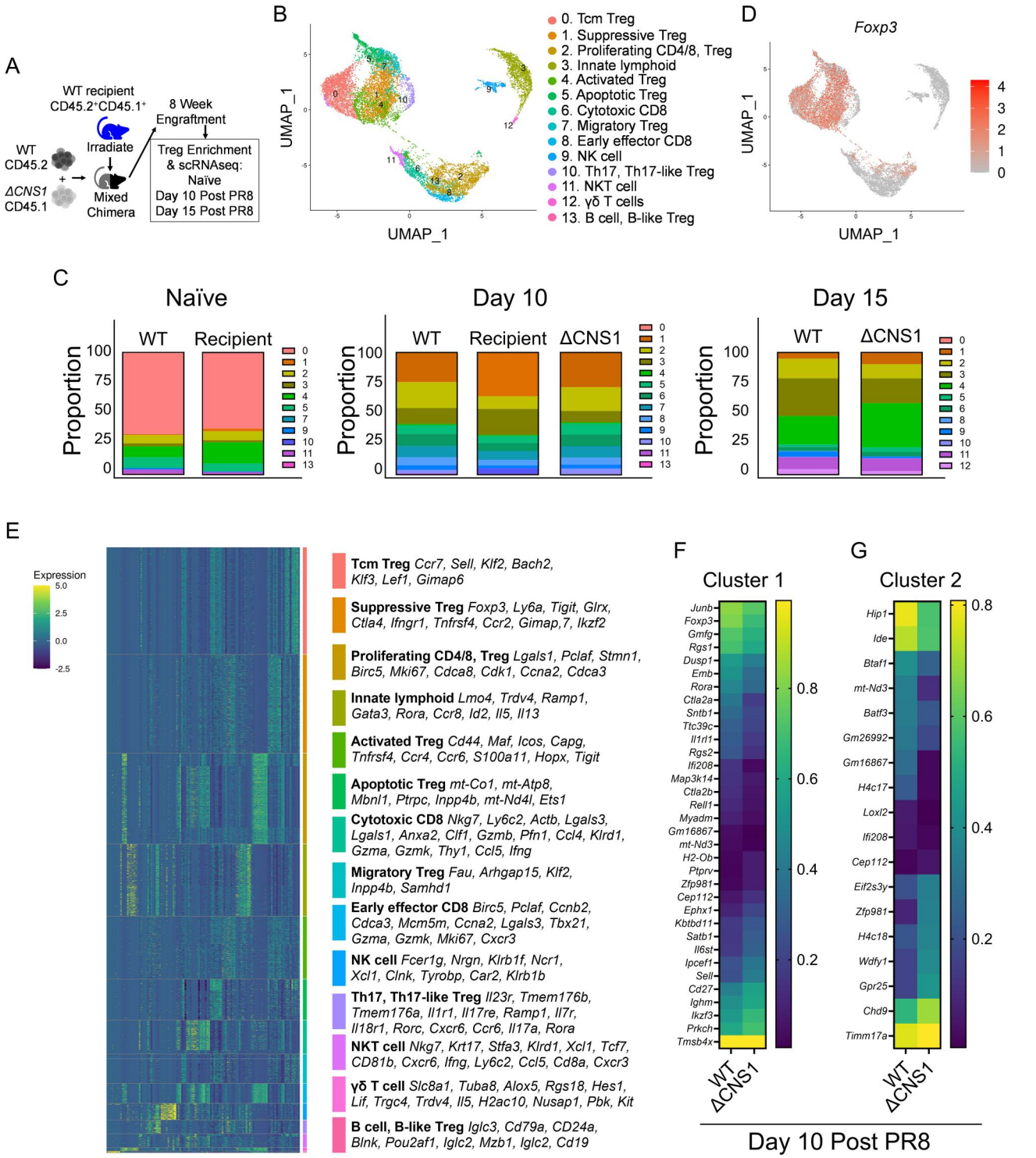

Figure 6 scRNAseq reveals distinct Treg clusters throughout PR8-induced lung injury. (A) Adoptive transfer schematic for scRNAseq studies. (B) Overall clusters identified across time points and donor sources. (C) Cell clusters broken up by time point and by donor type. (D) *Foxp3* expression (red) across clusters. (E) Cluster identification by gene expression, with selected signature genes driving each cluster listed. (F, G) Presentation of expression levels in WT (left) and ΔCNS1 (right) cells from cluster 1 (F) and cluster 2 (G), 10 d post-PR8. Transcripts shown were identified as significantly differentially expressed.

differentiation, and activation signatures in WT cells, indicating that ΔCNS1 Tregs may be less well suited to a tissue-specific response to an inflammatory challenge in the lung.

When considering cluster 2 (proliferating $CD4^+/8^+$, Tregs), we observe several significant DEGs at day 10 post-PR8 (Fig. 6G). Many DEGs were related to chromatin structure, DNA binding,

and transcription, with several being upregulated in ΔCNS1 cells (*H4c18*, *Zfp981*, *Chd9*) and several being downregulated in ΔCNS1 cells (*Hc417*, *Batf1*, *Batf3*). Several genes involved in viral response (*Hip1* and *Ifi208*)[79,91] were also downregulated in ΔCNS1 cells. Other genes related to proinflammatory signaling were also upregulated in ΔCNS1 cells (*Gpr25*, *Wdfy1*).[92,93] Finally, several genes related to proliferation (*Eif2s3y* and *Cep112*)[94,95] were upregulated in ΔCNS1 cells. In this cluster on day 15 post-PR8, we observe 2 DEGs between WT and ΔCNS1 cells. These DEGs include *Emb* and *H4c17*, both of which were downregulated in ΔCNS1 compared with WT. *Emb* encodes an adhesion molecule involved in cell–extracellular matrix interactions. In pancreatic cancer, silencing Embigin (the protein derived from *Emb*) results in decreased cell proliferation, migration, invasion, and wound healing.[87]

Across subsets and the first two time points, recipient cells, identified by coexpression of CD45.1$^+$ and CD45.2$^+$, express elevated T central memory transcriptional signatures (*Sell*, *Ccr7*, *Klf2*, *Klf3*) and elevated genes related to TCR signaling (*Stat5b*, *Junb*, *Fos*). Combined with immunophenotyping data, we hypothesize that the remaining recipient Tregs following irradiation and reconstitution are tissue-resident Tregs that maintain activation and TCR stimulation, and that they proliferate following ALI.

Single-cell transcriptomic profiling revealed that CNS1 deletion disrupts the normal differentiation trajectories of Tregs following influenza-induced lung injury. ΔCNS1 Tregs, when compared with WT Tregs, demonstrated diminished expression of tissue-adaptive and repair-associated genes (*Rora*, *Ctla2a*, *Emb*, *Ifi208*) and enhanced naïve or early effector signatures, indicating that loss of CNS1 impairs Treg polarization toward reparative and tissue-resident phenotypes required for optimal Treg-directed recovery from lung injury.

CNS1 influences the TCR repertoire

To further understand the role of CNS1 in the response to PR8-induced ALI, we subjected cells from single-cell RNA sequencing (scRNAseq) analyses to TCRseq. We identified clones across most clusters with varying levels of clonality (Fig. 7A) and were able to detect clones from all donor/recipient sources (Fig. 7B). When considering cells in cluster 2 (see Fig. 6B, D for reference), we observe that among the *Foxp3*-expressing cells in this cluster, medium clones originate from CD45.2$^+$ (WT) cells only (Fig. 7C). Small *Foxp3*-expressing clones in this cluster have the most contributions from CD45.1$^+$ CD45.2$^+$ (recipient) cells (48.19%), followed by CD45.2$^+$ (WT) cells (33.70%), and CD45.1$^+$ (ΔCNS1) cells (18.11%) (Fig. 7C). While most clones from *Foxp3*-expressing cells in cluster 2 originate from small clones (97.6%), we speculate that the medium clones may represent a subset of CD4$^+$ cells susceptible to peripheral induction of Foxp3 via CNS1, which could contribute to the resolution of inflammation and tissue recovery in ALI. Further evidence for this hypothesis comes from observations of clonal overlap between *Foxp3*$^+$ and *Foxp3*$^-$ cells that fall into cluster 2 on day 15 post-PR8. By analyzing CTstrict sequences (a combination of V, D, J genes in the TCRα and TCRβ and the nucleotide sequence for the CDR3 region) and excluding incomplete data, we find clonal overlap between *Foxp3*$^+$ and *Foxp3*$^-$ cells in WT but not ΔCNS1 cells (Fig. 7D). Analysis of expression of Treg genes of interest among the 127 *Foxp3*-expressing day 15 cluster 2 cells reveals that ΔCNS1 Tregs show increased expression of transcription factors and molecules that exert suppressive function (Fig S10C). These genes include *Foxp3*, *Il2ra*, *Ctla4*, *Tigit*, *Tgfb1*, *Ezh2*, *Izkf2*, *Nr4a1*, and *Junb*. *Satb1* is also upregulated in ΔCNS1 Tregs, indicative of Treg dysfunction.[96] Genes demonstrating decreased expression in ΔCNS1 Tregs include *Pdcd1* (encodes PD-1), *Ebi3* (IL-35), *Nt5e* (CD73), *Il1rl1* (ST-2), and *Fos* (Fig. S10C). Previous studies have found that intratumoral Tregs are induced with Fos-mediated expression of PD-1.[97] IL-35 expression also induces the Treg fate, and IL-35-induced Tregs are potently suppressive and are producers of IL-35 themselves.[98] As mentioned before, CD73 expression contributes to a suppressive metabolic microenvironment.[42] These results indicate that while the Tregs in cluster 2 from ΔCNS1 mice may express more classic Treg functional transcription factors and molecules, there are various genetic tissue adaptations governed either directly or indirectly by CNS1.

Figure 7E depicts Morisita-Horn indices to compare TCR repertoires across identified cell populations in the scRNAseq data by time point (naïve, day 10 post-PR8, or 15 post-PR8), and cell source (recipient, WT donor, or ΔCNS1 donor). Overall, the ΔCNS1 and WT donor cells are more dissimilar to one another (Morisita index = 0.016) at day 10 than they are to the recipient population (ΔCNS1 day 10 versus recipient day 10 = 0.039; WT day 10 versus recipient day 10 = 0.037). Overall, little similarity was observed between populations, with the most notable overlap occurring on day 10 post-PR8.

TCR repertoire analysis revealed that CNS1 influences the clonal dynamics of Foxp3$^+$ T cells following influenza-induced lung injury. While Foxp3$^+$ cells in cluster 2 were primarily composed of small clones from all genotypes, medium-sized clones were uniquely derived from WT cells, consistent with CNS1-dependent peripheral Treg induction. Global TCR similarity analyses revealed minimal overlap between populations, with the greatest convergence observed at day 10 postinfection in donor-recipient comparisons. Notably, more divergence was seen between ΔCNS1 and WT donors compared with the remaining recipient cells at day 10 postinfection, indicating distinct clonal responses shaped by CNS1 during the peak of lung inflammation. Table S5C lists all TCRseq metadata.

Discussion

Prior comparative sequence analysis of the CNS1 region has shown that CNS1 is a mammalian-specific acquisition restricted to eutherian mammals, which evolved in response to the need for maternal tolerance of the fetus.[25,99] Additionally, in vitro and in vivo suppression assays with splenic and lymph node-derived Tregs from ΔCNS1 mice do not reveal defects in suppressive function.[26] Herein we show that the presence of the CNS1 region in the *Foxp3* locus, which induces Foxp3 expression in peripheral CD4$^+$ T cells, is crucial for optimal Treg mechanisms that promote recovery and survival from ALI. Foxp3-independent mechanisms for pTreg induction have been reported,[54] supporting that ΔCNS1 mice still retain the ability to generate pTregs. Furthermore, pTregs have been reported to develop in ΔCNS1

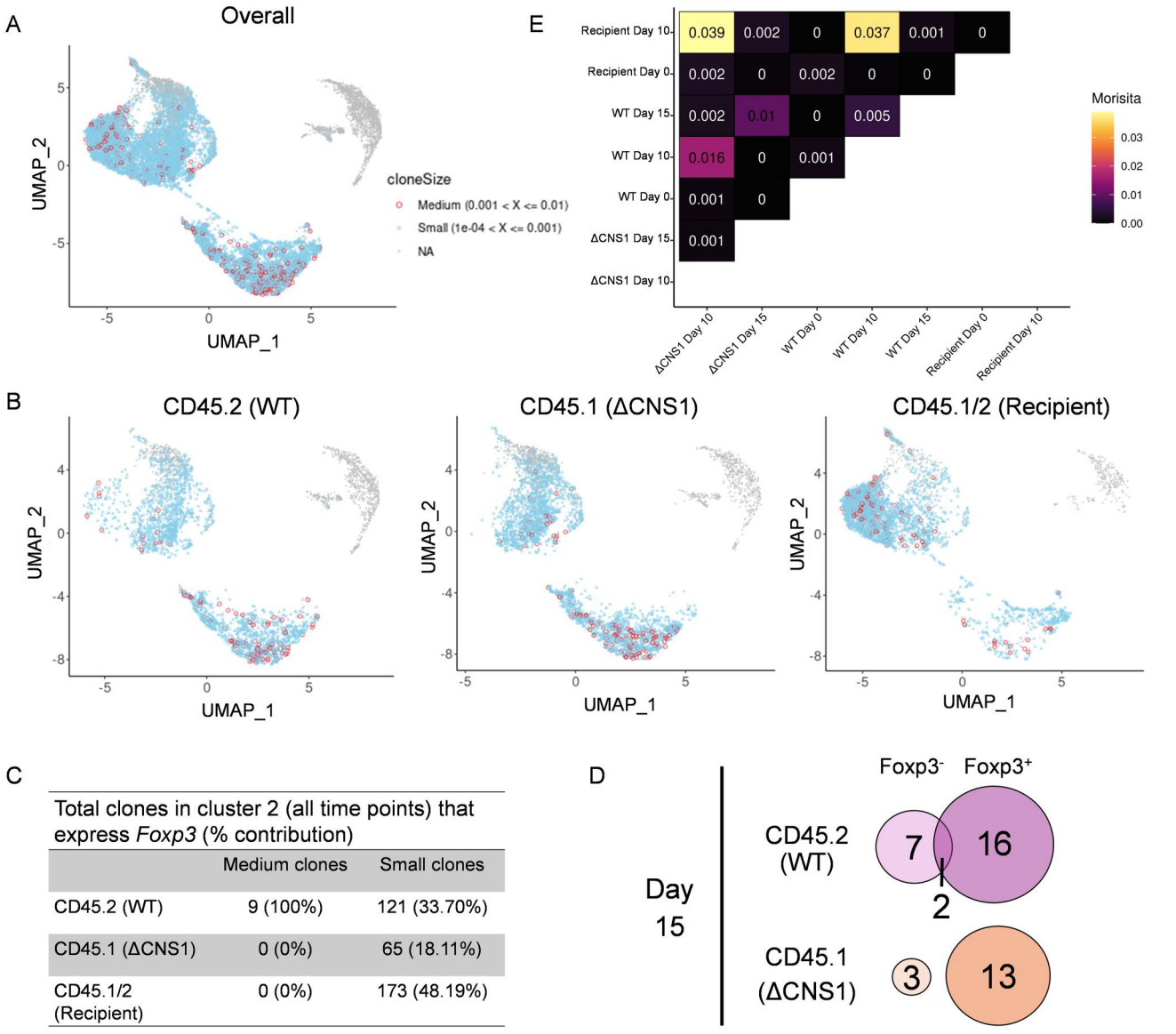

Figure 7 Clonal architecture of T cells revealed by TCRseq across genotypes and time points. (A) Overall clones from all donors at all time points. (B) Clones identified from WT (left), ΔCNS1 (middle), and recipient (right) cells. Red circles indicate a higher degree of clonal expansion than blue dots. (C) Total clones in cluster 2 from all time points (proliferating CD4, CD8 effector T cells, proliferating Tregs) derived from cells that express *Foxp3*. (D) Number of distinct clones (CTstrict) detected in cluster 2 at day 15 post-PR8 in $Foxp3^+$ and $Foxp3^-$ cells, with clonal overlap shown. Number inside circle represents number of distinct clones. (E) Clonal overlap (Morisita-Horn index) between WT, ΔCNS1, and recipient cells at steady state (day 0), day 10 post-PR8, or day 15 post-PR8. NA, cells lacking clonotype information.

mice following prolonged antigen exposure in the intestine.[21] Nevertheless, we observe an acute, nonredundant role for CNS1 in regulating immune infiltration into the alveolar space, immune cell activation, and lung epithelial recovery in ALI. This suggests that the Tregs induced by *Foxp3* induction via CNS1 in $CD4^+$ T cells play a role in controlling immune cell infiltration, activation, and tissue repair during ALI. Unlike previous reports,[26] we do not observe overt spontaneous inflammation in the naïve lung tissue of ΔCNS1 mice, potentially due to differences in housing facilities and associated exposomes. Our results build on those showing that ex vivo inducible Tregs facilitate ALI recovery[100] but are the first to show that CNS1 has a nonredundant role in pTreg induction in the lung during ALI. Furthermore, we show that contrary to previous reports of CNS1 being important for control of Th2 responses,[26] CNS1 is important in controlling a the largely Th1-driven disease process of PR8-induced ALI, providing evidence for the hypothesis that the role of CNS1 may be context dependent.

While Treg numbers in the lungs of ΔCNS1 mice increase following ALI, the expansion is significantly blunted compared with that observed in WT mice. This suggests that multiple mechanisms may contribute to the increased Treg numbers observed in WT mice. However, our studies show that Treg induction via CNS1 contributes significantly to the increase in Tregs observed in the lungs following ALI. Increased Foxp3 expression was observed in Tregs of naïve and day 15 post-PR8 ΔCNS1 mice. Foxp3 expression levels have previously been linked to Treg stability.[101] Additionally, expression of functional markers by Tregs

also differs in ΔCNS1 mice. ΔCNS1 Tregs are more likely to express CD103, CD73, and IL-10, indicating that these Treg functions may be enriched in thymically derived Tregs. Helios (*Ikzf2*), a disputed marker of thymically derived Tregs,[39,41,102] is elevated in ΔCNS1 Tregs. While we do not demonstrate that Helios is a bona fide marker for thymically derived Tregs, our results contribute to the evidence that Helios is a marker of Treg stability, as Helios and Foxp3 expression are linked,[47,48] and both are elevated in ΔCNS1 Tregs. We also report nonredundant roles for Helios$^-$ Tregs in expressing markers associated with TGF-β signaling in Tregs, previously shown to be associated with ALI recovery[6] as well as *Foxp3* induction via inducing Smad3 to bind to CNS1.[27,28] Our results align with previous studies that have highlighted differences between Helios$^+$ and Helios$^-$ Tregs, both in their TCR specificity and functionality.[103] Furthermore, Helios$^-$ Tregs are also more likely to be CD44$^+$, indicating sustained TCR activation, which previous reports have found sustains *Foxp3* expression via NFAT.[28] ΔCNS1 Tregs also exhibit decreased expression of IL-13 and GATA3, which represent Treg markers associated with controlling innate inflammation.[5,8,10] These findings support a role for the CNS1 enhancer in facilitating the generation of peripherally induced Tregs that can adapt to local environmental cues. This adaptive capacity, often referred to as Treg plasticity—the ability to modify functional programs in response to the tissue environment—is shaped by mechanisms governing peripheral Treg differentiation. Thus, the CNS1 locus, which mediates peripheral induction of Foxp3$^+$ Tregs, may be a key determinant of this plasticity, enabling the generation of Tregs that acquire Th-like traits while maintaining their suppressive function.

CNS1 loss also influences B cell development following ALI, perhaps by reducing Tfh cell induction. This result, along with decreased GATA3 positivity in ΔCNS1 effector T cells following ALI, indicates that low-level *Foxp3* expression via CNS1 could skew the effector CD4$^+$ T cell response without inducing the Treg fate, or that Tregs induced by CNS1 contribute to modulating effector T cell skewing. We also observe a decrease in Tfr cell numbers in CNS1 mice. Tfr cells function to fine-tune GC processes.[104] However, Tfr cells as a percentage of total Tregs are not decreased in CNS1 mice, suggesting that fewer Tfr cells may result from decreased Tfh cells. While Tfr cells are thought to be of thymic origin,[105] a subset of CD4$^+$ Tfh cells that transiently express Foxp3 has been reported to direct GC dynamics.[52] This indicates that low-level, transient Foxp3 expression may facilitate the fine-tuning of the immune response during ALI resolution. Still, these observations regarding Tfh and Tfr cells do not result in changes in total GC B cells (as previously observed in CNS1 mice)[26]; however, we do observe decreased MHCII expression in GC B cells, which may indicate impaired GC B cell function. While we do observe aberrant local (BAL) and systemic (serum) antibody production at baseline and throughout injury in ΔCNS1 mice, we do not observe an impaired ability of ΔCNS1 mice to produce a PR8-specific antibody. The contributions of autoantibodies to ALI pathology remain unclear, as ΔCNS1 mice display elevated baseline autoantibody levels, a phenotype that differs less from WT autoantibody levels as injury progresses. Previous reports have identified autoreactive antibodies in ΔCNS1 mice,[26] and autoreactive T cells have been shown to contribute to autoimmune processes during ALI.[106] Recent work has identified that Tregs suppress self-reactive effector T cells with a shared TCR specificity during infection, allowing for a robust antipathogen T cell response while limiting autoreactive immune responses.[55] Future studies will identify the role of CNS1 in this process and assess the potential development of autoreactive effector T cells in ΔCNS1 mice. Autoreactive T cell and antibody responses may be important, as anecdotal reports suggest associations between infection and subsequent autoimmunity.[107] Additionally, respiratory infections can act as inciting events for deleterious autoimmune processes that influence the immune response during injury or later after the infection has resolved.[108]

The development of Tregs with TCRs reactive to the PR8 NP tetramer was significantly impaired in ΔCNS1 mice, without adversely affecting the development of CD4$^+$ and CD8$^+$ PR8 NP tetramer reactivity, indicating that the loss of CNS1 does not affect effector T cell TCR development. Indeed, at day 10 post-PR8, we found a higher total number of NP-reactive CD4$^+$ effector T cells in ΔCNS1 mice than in WT mice, suggesting a potential accumulation of effector T cells that are unable to become Tregs. The lack of difference in NP-reactive CD4$^+$ effector T cells at day 15 could be explained by survivor bias. When considering tetramer-reactive Tregs from wild-type mice, we found that Foxp3 and Helios expression were lower in this subset, consistent with a previous report of mice infected with human metapneumovirus.[14] NP-reactive Tregs have significantly elevated expression of Ki-67, Ccr4, and CXCR3. Further, in our TCRseq analyses of WT, recipient, and ΔCNS1 cells, we found that among proliferating cells (cluster 2), those *Foxp3*-expressing cells with medium clone sizes (i.e. are more clonal) come exclusively from WT cells, which could indicate proliferating CD4$^+$ effector T cells are becoming *Foxp3*-expressing cells only in this group. When considering cluster 2 at day 15, we also find TCR clonal overlap between *Foxp3*$^+$ and *Foxp3*$^-$ cells in WT but not ΔCNS1 cells, further suggesting shared lineage among WT Tregs and non-Tregs that is lost when CNS1 is deleted. Expression of Treg effector genes and transcription factors in *Foxp3*-expressing cells of cluster 2 at day 15 also reveal that CNS1 Tregs fail to induce transcriptional programs resulting from antigen stimulation, TCR signaling, and tissue adaptation.[42,96–98] Overall, these results support the hypothesis that Th1-like Tregs (reported by others in ALI and in other disease states)[5,109] arise from Th1 effector cells with NP-reactive TCRs, where they no longer cause Th1 pathology that contributes to mortality from influenza and may also be better positioned to exert their suppressive and/or tissue reparative functions. This process may represent many subsets of Th1 cells with TCRs specific to various antigens involved in ALI and could contribute to the increased mortality observed in ΔCNS1 mice. While we do detect low-level induction of Foxp3 in transferred CD4$^+$ T cells, future fate-mapping studies are needed to provide additional support for the previously mentioned hypothesis. Transferring CD4$^+$ effector T cells from WT mice partially rescues mortality in ΔCNS1 mice, indicating that CNS1 directs a supportive function of effector T cells, but more studies are needed to better describe this process. Previous reports in the gut have found that over time, ΔCNS1 mice do develop Tregs specific to non–self-antigens; however, this process is significantly delayed.[21] Together, these results indicate that CNS1-

mediated Treg induction may be more important in severe acute inflammatory events than in chronic conditions.

Identifying relevant, shared TCRs across ALI could guide targeted Treg therapies for ARDS and other diseases in which Treg-mediated immunomodulation and tissue repair are crucial. To date, two polyclonal Treg therapy trials have been conducted for acute respiratory distress syndrome resulting from severe COVID-19 infection (NCT04468971; NCT05027815). One study has been published and demonstrated safety, and the other was terminated due to low enrollment.[110] Our results suggest that peripheral Treg induction to pathogenic antigens may, in part, contribute to the enhancement of Treg function in ARDS. Future trials evaluating allogeneic Treg therapy from donors with prior infection or vaccination may be more effective than those from donors not previously exposed.

In chimeric mice, engraftment following bone marrow and splenocyte resulted in an overrepresentation of ΔCNS1 $CD8^+$ T cells, $CD4^+$ T cells, and Tregs measured by flow cytometry. We do not establish a mechanism for this phenomenon. However, we speculate that this could be due to increased expression of CD103, a tissue-retention marker and integrin molecule, on ΔCNS1 Tregs, which subsequently supports the retention of effector T cells to a greater degree. What is clear, however, is that WT donor cells outcompete ΔCNS1 cells as ALI progresses, indicating that WT cells may have higher fitness or a greater ability to control inflammation than ΔCNS1 cells. In chimeric mice, we observe, as others have summarized,[111] that Tregs are radioresistant in irradiated recipient mice and that a subset of recipient Tregs remains following irradiation, which then expands during ALI. At the same time, we detect very few recipient $CD4^+$ and $CD8^+$ effector T cells following irradiation and reconstitution, as well as when chimeric mice are exposed to PR8. We hypothesize that these recipient tissue-resident Tregs have TCRs specific for self-antigens and play a protective role following ALI. To this point, recipient cells expressed elevated *Il7r*, likely indicating that these cells are more responsive to IL-7 released by recipient lung tissue,[112] which may drive the proliferation observed in this subset.

In chimeric mice, we observed several cell-intrinsic phenotypes of ΔCNS1 Tregs (Foxp3 expression, Helios positivity, CD103 positivity, IFNγ positivity, CD44 expression) and several Treg phenotypes that do not persist in chimeric mice (IL-10 positivity, CD73 positivity, GARP positivity, LAP positivity). These different outcomes may be a result of a more heterogeneous immune environment, in which ΔCNS1 Tregs could diverge from their nonchimeric phenotype due to signals from WT Tregs that they did not receive in nonchimeric mice, or due to the loss of necessity for compensatory effects in a chimeric mouse, in which WT Tregs are present to provide optimal function. ΔCNS1 × *Foxp3*^{DTR} heterozygote female mice further reveal compensatory control of Th1 cytokines in whole-body ΔCNS1 mice, and frame CNS1 as a mechanism that Tregs use to perform the crucial function of suppressing Th1 inflammation in ALI.[113]

The scRNAseq analysis of Tregs throughout ALI revealed the emergence of a critical subset (cluster 1) of Tregs that likely contain pTregs due to elevated expression of *Foxp3*, *Rora*, and *Ctla2a* in WT Tregs compared with ΔCNS1 Tregs. We hypothesize that this cluster represents a previously unresolved population of cells that shows Treg phenotypes not observed in flow cytometry analysis of chimeric Tregs (marked by Foxp3 expression). A key DEG in this subset included *Il1rl1*. Considering our findings that $Ly6C^+$ macrophages are increased in nonchimeric ΔCNS1 mice (Fig. 1G), as well as the fact that IL-6, G-CSF, KC, and MCP-1 were elevated in BALF from ΔCNS1 mice (Table S2), we postulate that CNS1-induced pTregs (or a subset of pTregs) express ST-2 (as evidenced by decreased *Il1r1* transcripts in ΔCNS1 Tregs in cluster 1) and IL-13, which have previously been shown to enhance resolution of ALI through modulating proinflammatory macrophage responses by decreasing IL-6, G-CSF, and MCP-1, and Ly6C-hi monocyte-derived macrophages.[8,10] These results further align with what we observe in nonchimeric ΔCNS1 Tregs, as decreased Treg IL-13 production is observed in ΔCNS1 Tregs (Fig. 2H). Notably, all these differences were detected at day 10 post-PR8, a time point at which we observe divergence in mortality rates between nonchimeric ΔCNS1 and WT mice, suggesting that CNS1 may play a role in Treg function early in the injury process. We believe our results are translationally relevant, as IL-6 is associated with severe lung injury[114] and IL-6 receptor blockade is a treatment for severe COVID-19–associated ARDS.[115] Our results further support exploration of $ST\text{-}2^+$ Tregs as a therapeutic avenue for severe ARDS.

These results, in tandem with our results regarding the radioresistant recipient Tregs in the chimeric model, paint a complex picture of multiple Treg subsets from distinct sources with distinct phenotypes that may direct the diverse functions of Tregs in ALI recovery.

Our study identifies CNS1-dependent Foxp3 induction as a critical driver of Treg responses that control immune infiltration, promote lung repair, and improve survival in ALI. Although ΔCNS1 mice can generate Tregs, they fail to exhibit pathogen-specific, plastic, and functionally active Treg subsets during acute inflammation, leading to dysregulated Treg-specific immune function and poorer outcomes. These findings highlight CNS1 as a key driver of Treg heterogeneity and fitness in acute settings, suggesting that leveraging pTreg induction via CNS1 may enhance the efficacy of emerging Treg-based therapies for ARDS and related inflammatory diseases.

Acknowledgments

We thank Dr. Alexander Rudensky for providing the CNS1-deficient mice (*Foxp3*$^{\Delta CNS1-gfp}$ mice)[25] and Dr. Nicholas Heaton for advising the PR8-specific antibody ELISA assays. We also thank the National Institutes of Health Tetramer Core Facility (National Institutes of Health Contract 75N93020D00005 and RRID: SCR_026557) for providing H2-Db Influenza A NP 366-374 ASNENMETM Brilliant Violet 421-Labeled Tetramer (cat. #75812), I-Ab Influenza A NP 311-325 QVYSLIRPNENPAHK Brilliant Violet 421-Labeled Tetramer (cat. #76637), H2-Db Human gp100 25-33 KVPRNQDWL Brilliant Violet 421-Labeled Tetramer (cat. #75813), and I-A(b) human CLIP 87-101 PVSKMRMATPLLMQA Brilliant Violet 421-Labeled Tetramer (cat. #76638). Clinical Chemistry was performed within the Department of Pathology, Animal Clinical Chemistry Core at the University of North Carolina at Chapel Hill. The University of Texas Southwestern Microarray and Immune Phenotyping Core analyzed serum samples for autoantibodies.

Author contributions

M.J.M. (Conceptualization [Equal], Data curation [Lead], Formal analysis [Lead], Investigation [Lead], Methodology [Equal], Writing—original draft [Lead], Writing—review & editing [Equal]), M.K.T. (Investigation [Equal], Methodology [Equal], Project administration [Equal], Writing—review & editing [Equal]), J.W.G. (Investigation [Equal], Methodology [Equal], Writing—review & editing [Equal]), B.L.B. (Investigation [Equal], Writing—review & editing [Equal]), M.H. (Investigation [Equal], Methodology [Equal], Writing—review & editing [Equal]), Y.F. (Funding acquisition [Supporting], Investigation [Equal], Methodology [Equal], Writing—review & editing [Equal]), B.V. (Methodology [Equal], Writing—review & editing [Equal]), J.J.M. (Investigation [Equal], Supervision [Equal], Writing—review & editing [Equal]), A.T. (Investigation [Equal], Supervision [Equal], Writing—review & editing [Equal]), Y.Y.W. (Investigation [Equal], Supervision [Equal], Writing—review & editing [Equal]), H.D. (Conceptualization [Equal], Data curation [Equal], Formal analysis [Equal], Methodology [Equal], Writing—review & editing [Equal]), and C.D. (Funding acquisition [Supporting], Investigation [Equal], Resources [Equal], Writing—review & editing [Equal]), J.R.M. (Conceptualization [Equal], Data curation [Equal], Formal analysis [Equal], Funding acquisition [Lead], Investigation [Equal], Methodology [Equal], Resources [Equal], Supervision [Lead], Writing—original draft [Supporting], Writing—review & editing [Lead])

Supplementary material

Supplementary material is available at *The Journal of Immunology* online.

Funding

M.J.M. was supported through the American Association of Immunologists Careers in Immunology Fellowship Program. The National Heart, Lung, and Blood Institute of the National Institutes of Health supported J.R.M.'s research (R01HL152077 and R01HL173765). This study was also supported by the American Lebanese Syrian Associated Charities (St. Jude Children's Research Hospital); National Institutes of Health grants R21 AI163942 (Y.F.), R01 AI153138 (Y.F.), R01 HL145396 (C.M.D.), and R01HL175463 (C.M.D.); and National Cancer Institute Cancer Center support grant P30 CA021765 (St. Jude Children's Research Hospital).

Conflicts of interest

The authors declare that they have no conflict of interest.

Data availability

Multiomic scRNAseq data reported in this paper have been deposited in the Gene Expression Omnibus (https://www.ncbi.nlm.nih.gov/geo/) under accession code GSE300399. This study does not report the original code. The data underlying this article will be shared on reasonable request to the corresponding author.

References

1. McCullough MJ, Bose PG, Mock JR. Regulatory t cells: supporting lung homeostasis and promoting resolution and repair after lung injury. Int J Biochem Cell Biol. 2024;170:106568.
2. Jovisic M, Mambetsariev N, Singer BD, Morales-Nebreda L. Differential roles of regulatory t cells in acute respiratory infections. J Clin Invest. 2023;133:e170505.
3. Kim JM, Rasmussen JP, Rudensky AY. Regulatory t cells prevent catastrophic autoimmunity throughout the lifespan of mice. Nat Immunol. 2007;8:191–197.
4. D'Alessio FR, Kurzhagen JT, Rabb H. Reparative t lymphocytes in organ injury. J Clin Invest. 2019;129:2608–2618.
5. Griffith JW et al. Regulatory t cell-derived il-1ra suppresses the innate response to respiratory viral infection. Nat Immunol. 2023;24:2091–2107.
6. D'Alessio FR et al. Cd4+cd25+foxp3+ tregs resolve experimental lung injury in mice and are present in humans with acute lung injury. J Clin Invest. 2009;119:2898–2913.
7. Mock JR et al. Transcriptional analysis of foxp3+ regulatory t cells and functions of two identified molecules during resolution of ali. JCI Insight. 2019;4:e124958.
8. Proto JD et al. Regulatory t cells promote macrophage efferocytosis during inflammation resolution. Immunity. 2018;49:666–677.e6.
9. Aggarwal NR et al. Immunological priming requires regulatory t cells and il-10-producing macrophages to accelerate resolution from severe lung inflammation. J Immunol. 2014;192:4453–4464.
10. Liu Q et al. Il-33–mediated il-13 secretion by st2+ tregs controls inflammation after lung injury. JCI Insight. 2019;4:e123919.
11. Xu R et al. Tnfr2+ regulatory t cells protect against bacteremic pneumococcal pneumonia by suppressing il-17a-producing γδ t cells in the lung. Cell Rep. 2023;42:112054.
12. Betts RJ et al. Influenza a virus infection results in a robust, antigen-responsive, and widely disseminated foxp3+ regulatory t cell response. J Virol. 2012;86:2817–2825.
13. Ruckwardt TJ, Bonaparte KL, Nason MC, Graham BS. Regulatory t cells promote early influx of cd8+ t cells in the lungs of respiratory syncytial virus-infected mice and diminish immunodominance disparities. J Virol. 2009;83:3019–3028.
14. Rogers MC et al. Cd4(+) regulatory t cells exert differential functions during early and late stages of the immune response to respiratory viruses. J Immunol. 2018;201:1253–1266.
15. Fulton RB, Meyerholz DK, Varga SM. Foxp3+ cd4 regulatory t cells limit pulmonary immunopathology by modulating the cd8 t cell response during respiratory syncytial virus infection. J Immunol. 2010;185:2382–2392.
16. Mock JR et al. Foxp3+ regulatory t cells promote lung epithelial proliferation. Mucosal Immunol. 2014;7:1440–1451.
17. Kaiser KA, Loffredo LF, Santos-Alexis KL, Ringham OR, Arpaia N. Regulation of the alveolar regenerative niche by

amphiregulin-producing regulatory t cells. J Exp Med. 2023; 220:e20221462.
18. Garibaldi BT et al. Regulatory t cells reduce acute lung injury fibroproliferation by decreasing fibrocyte recruitment. Am J Respir Cell Mol Biol. 2013;48:35–43.
19. D'Alessio FR, Zhong Q, Jenkins J, Moldobaeva A, Wagner EM. Lung angiogenesis requires cd4(+) forkhead homeobox protein-3(+) regulatory t cells. Am J Respir Cell Mol Biol. 2015;52:603–610.
20. Wiesner DL et al. Regulatory t cell induction and retention in the lungs drives suppression of detrimental type 2 th cells during pulmonary cryptococcal infection. J Immunol. 2016;196:365–374.
21. Nutsch K et al. Rapid and efficient generation of regulatory t cells to commensal antigens in the periphery. Cell Rep. 2016;17:206–220.
22. Lathrop SK et al. Peripheral education of the immune system by colonic commensal microbiota. Nature. 2011; 478:250–254.
23. Kim KS et al. Dietary antigens limit mucosal immunity by inducing regulatory t cells in the small intestine. Science. 2016;351:858–863.
24. Campbell C et al. Extrathymically generated regulatory t cells establish a niche for intestinal border-dwelling bacteria and affect physiologic metabolite balance. Immunity. 2018;48:1245–1257.e9.
25. Zheng Y et al. Role of conserved non-coding DNA elements in the foxp3 gene in regulatory t-cell fate. Nature. 2010; 463:808–812.
26. Josefowicz SZ et al. Extrathymically generated regulatory t cells control mucosal th2 inflammation. Nature. 2012; 482:395–399.
27. Schlenner SM, Weigmann B, Ruan Q, Chen Y, von Boehmer H. Smad3 binding to the foxp3 enhancer is dispensable for the development of regulatory t cells with the exception of the gut. J Exp Med. 2012;209:1529–1535.
28. Tone Y et al. Smad3 and nfat cooperate to induce foxp3 expression through its enhancer. Nat Immunol. 2008; 9:194–202.
29. Lee W, Lee GR. Transcriptional regulation and development of regulatory t cells. Exp Mol Med. 2018;50:e456.
30. Mock JR, Tune MK, Bose PG, McCullough MJ, Doerschuk CM. Comparison of different methods of initiating lung inflammation and the sex-specific effects on inflammatory parameters. Am J Physiol Lung Cell Mol Physiol. 2023; 324:L199–L210.
31. Zhu H, Luo H, Yan M, Zuo X, Li Q-Z. Autoantigen microarray for high-throughput autoantibody profiling in systemic lupus erythematosus. Genomics Proteomics Bioinformatics. 2015;13:210–218.
32. Yang Q, Safina KR, Nguyen KDQ, Tuong ZK, Borcherding N. Screpertoire 2: Enhanced and efficient toolkit for single-cell immune profiling. PLoS Comput Biol. 2025;21:e1012760.
33. Germain PL, Lun A, Garcia Meixide C, Macnair W, Robinson MD. Doublet identification in single-cell sequencing data using scdblfinder. F1000Res. 2021;10:979.
34. Hao Y et al. Dictionary learning for integrative, multimodal and scalable single-cell analysis. Nat Biotechnol. 2024; 42:293–304.
35. Borcherding N, Bormann NL, Kraus G. Screpertoire: an r-based toolkit for single-cell immune receptor analysis. F1000Res. 2020;9:47.
36. Lee S, Margolin K. Cytokines in cancer immunotherapy. Cancers (Basel). 2011;3:3856–3893.
37. Colamatteo A et al. Molecular mechanisms controlling foxp3 expression in health and autoimmunity: From epigenetic to post-translational regulation. Front Immunol. 2019;10:3136.
38. Plitas G, Rudensky AY. Regulatory t cells: differentiation and function. Cancer Immunol Res. 2016;4:721–725.
39. Thornton AM et al. Expression of helios, an ikaros transcription factor family member, differentiates thymic-derived from peripherally induced foxp3+ t regulatory cells. J Immunol. 2010;184:3433–3441.
40. Gottschalk RA, Corse E, Allison JP. Expression of helios in peripherally induced foxp3+ regulatory t cells. J Immunol. 2012;188:976–980.
41. Szurek E et al. Differences in expression level of helios and neuropilin-1 do not distinguish thymus-derived from extrathymically induced cd4+foxp3+ regulatory t cells. PLoS One. 2015;10:e0141161.
42. Da M, Chen L, Enk A, Ring S, Mahnke K. The multifaceted actions of cd73 during development and suppressive actions of regulatory t cells. Front Immunol. 2022; 13:914799.
43. Kitz A, Dominguez-Villar M. Molecular mechanisms underlying th1-like treg generation and function. Cell Mol Life Sci. 2017;74:4059–4075.
44. Dikiy S, Rudensky AY. Principles of regulatory t cell function. Immunity. 2023;56:240–255.
45. Skadow M, Penna VR, Galant-Swafford J, Shevach EM, Thornton AM. Helios deficiency predisposes the differentiation of cd4(+)foxp3(-) t cells into peripherally derived regulatory t cells. J Immunol. 2019;203:370–378.
46. Singh K, Hjort M, Thorvaldson L, Sandler S. Concomitant analysis of helios and neuropilin-1 as a marker to detect thymic derived regulatory t cells in naïve mice. Sci Rep. 2015;5:7767.
47. Takatori H et al. Helios enhances treg cell function in cooperation with foxp3. Arthritis Rheumatol. 2015; 67:1491–1502.
48. Sebastian M et al. Helios controls a limited subset of regulatory t cell functions. J Immunol. 2016;196:144–155.
49. Zabransky DJ et al. Phenotypic and functional properties of helios+ regulatory t cells. PLoS One. 2012;7:e34547.
50. Lam AJ, Uday P, Gillies JK, Levings MK. Helios is a marker, not a driver, of human treg stability. Eur J Immunol. 2022; 52:75–84.
51. Chaurio RA et al. Tgf-β-mediated silencing of genomic organizer satb1 promotes tfh cell differentiation and formation of intra-tumoral tertiary lymphoid structures. Immunity. 2022;55:115–128.e119.
52. Jacobsen JT et al. Expression of foxp3 by t follicular helper cells in end-stage germinal centers. Science. 2021; 373:eabe5146.
53. Syeda MZ, Hong T, Huang C, Huang W, Mu Q. B cell memory: From generation to reactivation: a multipronged

defense wall against pathogens. Cell Death Discov. 2024; 10:117.
54. van der Veeken J et al. Genetic tracing reveals transcription factor foxp3-dependent and foxp3-independent functionality of peripherally induced treg cells. Immunity. 2022;55: 1173–1184.e7.
55. Klawon DEJ et al. Regulatory t cells constrain t cells of shared specificity to enforce tolerance during infection. Science. 2025;387:eadk3248.
56. Iamsawat S et al. Single-cell analysis uncovers striking cellular heterogeneity of lung-infiltrating regulatory t cells during eosinophilic versus neutrophilic allergic airway inflammation. J Immunol. 2024;212:1867–1876.
57. Zemmour D et al. Single-cell analysis of foxp3 deficiencies in humans and mice unmasks intrinsic and extrinsic cd4(+) t cell perturbations. Nat Immunol. 2021;22:607–619.
58. Liu X et al. Pclaf promotes neuroblastoma g1/s cell cycle progression via the e2f1/pttg1 axis. Cell Death Dis. 2022;13:178.
59. Rubin CI, Atweh GF. The role of stathmin in the regulation of the cell cycle. J Cell Biochem 2004;93:242–250.
60. Xu L, Yu W, Xiao H, Lin K. Birc5 is a prognostic biomarker associated with tumor immune cell infiltration. Sci Rep. 2021; 11:390.
61. Imbratta C et al. Maf deficiency in t cells dysregulates t(reg) - t(h)17 balance leading to spontaneous colitis. Sci Rep. 2019;9:6135.
62. McGee MC et al. Pd-1 and icos counter-regulate tissue resident regulatory t cell development and il-10 production during flu. Front Immunol. 2022;13:984476.
63. Galvan-Pena S et al. Profound treg perturbations correlate with covid-19 severity. Proc Natl Acad Sci U S A. 2021;118 (37):e2111315118.
64. Zemmour D et al. Single-cell gene expression reveals a landscape of regulatory t cell phenotypes shaped by the tcr. Nat Immunol. 2018;19:291–301.
65. Ding Y, Xu J, Bromberg JS. Regulatory t cell migration during an immune response. Trends Immunol. 2012; 33:174–180.
66. Saito K et al. Differential regulatory function of resting and preactivated allergen-specific cd4+cd25+ regulatory t cells in th2-type airway inflammation1. J Immunol. 2008; 181:6889–6897.
67. Yamazaki T et al. Ccr6 regulates the migration of inflammatory and regulatory t cells1. J Immunol. 2008; 181:8391–8401.
68. Osorio D, Cai JJ. Systematic determination of the mitochondrial proportion in human and mice tissues for single-cell rna-sequencing data quality control. Bioinformatics 2021;37:963–967.
69. Pabbisetty SK et al. Peripheral tolerance can be modified by altering klf2-regulated treg migration. Proc Natl Acad Sci USA 2016;113:E4662–E4670.
70. Sun Z et al. Forkhead box p3 regulates arhgap15 expression and affects migration of glioma cells through the rac1 signaling pathway. Cancer Sci. 2017;108:61–72.
71. Cuadrado E et al. Proteomic analyses of human regulatory t cells reveal adaptations in signaling pathways that protect cellular identity. Immunity. 2018;48:1046–1059.e6.
72. Baldauf H-M et al. Samhd1 restricts hiv-1 infection in resting cd4(+) t cells. Nat Med 2012;18:1682–1687.
73. Chen S et al. Samhd1 suppresses innate immune responses to viral infections and inflammatory stimuli by inhibiting the nf-κb and interferon pathways. Proc Natl Acad Sci U S A 2018;115:E3798–E3807.
74. Lee EJ et al. Single-cell rna sequencing reveals immuno-oncology characteristics of tumor-infiltrating t lymphocytes in photodynamic therapy-treated colorectal cancer mouse model. Int J Mol Sci. 2023;24:13913.
75. Crinier A et al. High-dimensional single-cell analysis identifies organ-specific signatures and conserved nk cell subsets in humans and mice. Immunity. 2018;49:971–986.e5.
76. Capone A et al. Systems analysis of human t helper17 cell differentiation uncovers distinct time-regulated transcriptional modules. iScience. 2021;24:102492.
77. Zhou L et al. Single-cell rna-seq analysis uncovers distinct functional human nkt cell sub-populations in peripheral blood. Front Cell Dev Biol. 2020;8:384.
78. Hu Y et al. Γδ t cells: origin and fate, subsets, diseases and immunotherapy. Signal Transduct Target Ther. 2023;8:434.
79. Cridland JA et al. The mammalian pyhin gene family: phylogeny, evolution and expression. BMC Evol Biol. 2012; 12:140.
80. Borghi R, Trivisano M, Specchio N, Tartaglia M, Compagnucci C. Understanding the pathogenetic mechanisms underlying altered neuronal function associated with camk2b mutations. Neurosci Biobehav Rev. 2023; 152:105299.
81. Sugita S et al. Induction of t regulatory cells by cytotoxic t-lymphocyte antigen-2α on corneal endothelial cells. Invest Ophthalmol Vis Sci. 2011;52:2598–2605.
82. Sun F et al. The mapk dual specific phosphatase (dusp) proteins: A versatile wrestler in t cell functionality. Int Immunopharmacol. 2021;98:107906.
83. Kishimoto T, Taga T, Akira S. Cytokine signal transduction. Cell 1994;76:253–262.
84. Delacher M et al. Single-cell chromatin accessibility landscape identifies tissue repair program in human regulatory t cells. Immunity. 2021;54:702–720.e17.
85. Borst J, Hendriks J, Xiao Y. Cd27 and cd70 in t cell and b cell activation. Curr Opin Immunol. 2005;17:275–281.
86. Malhotra N et al. Rorα-expressing t regulatory cells restrain allergic skin inflammation. Sci Immunol 2018;3:eaao6923.
87. Jung DE, Kim JM, Kim C, Song SY. Embigin is overexpressed in pancreatic ductal adenocarcinoma and regulates cell motility through epithelial to mesenchymal transition via the tgf-β pathway. Mol Carcinog. 2016;55:633–645.
88. Kim N et al. Unveiling the influence of tumor and immune signatures on immune checkpoint therapy in advanced lung cancer. Elife. 2024;13:RP98366.
89. Lippert DN, Wilkins JA. Glia maturation factor gamma regulates the migration and adherence of human t lymphocytes. BMC Immunol. 2012;13:21.
90. Powell MD, Read KA, Sreekumar BK, Oestreich KJ. Ikaros zinc finger transcription factors: Regulators of cytokine signaling pathways and cd4(+) t helper cell differentiation. Front Immunol. 2019;10:1299.

91. Jiang H, Sandoval Del Prado LE, Leung C, Wang D. Huntingtin-interacting protein family members have a conserved pro-viral function from caenorhabditis elegans to humans. Proc Natl Acad Sci U S A. 2020;117:22462–22472.
92. Hu YH et al. Wdfy1 mediates tlr3/4 signaling by recruiting trif. EMBO Rep. 2015;16:447–455.
93. Ocón B et al. A lymphocyte chemoaffinity axis for lung, non-intestinal mucosae and cns. Nature. 2024;635:736–745.
94. Liu W et al. Eif2s3y regulates the proliferation of spermatogonial stem cells via wnt6/<beta>-catenin signaling pathway. Biochim Biophys Acta Mol Cell Res. 2020;1867:118790.
95. Zhang X et al. Cep112 coordinates translational regulation of essential fertility genes during spermiogenesis through phase separation in humans and mice. Nat Commun. 2024;15:8465.
96. Beyer M et al. Repression of the genome organizer satb1 in regulatory t cells is required for suppressive function and inhibition of effector differentiation. Nat Immunol. 2011; 12:898–907.
97. Ma S et al. Serine enrichment in tumors promotes regulatory t cell accumulation through sphinganine-mediated regulation of c-fos. Sci Immunol. 2024;9:eadg8817.
98. Collison LW et al. Il-35-mediated induction of a potent regulatory t cell population. Nat Immunol. 2010;11:1093–1101.
99. Samstein RM, Josefowicz SZ, Arvey A, Treuting PM, Rudensky AY. Extrathymic generation of regulatory t cells in placental mammals mitigates maternal-fetal conflict. Cell. 2012;150:29–38.
100. Joudi AM et al. Maintenance DNA methylation is required for induced treg reparative function following viral pneumonia in mice. J Clin Invest. 2025;135:e192925.
101. Rudensky AY. Regulatory t cells and foxp3. Immunol Rev. 2011;241:260–268.
102. Pratama A, Schnell A, Mathis D, Benoist C. Developmental and cellular age direct conversion of cd4+ t cells into rorγ+ or helios+ colon treg cells. J Exp Med. 2020;217:e20190428.
103. Thornton AM et al. Helios(+) and helios(-) treg subpopulations are phenotypically and functionally distinct and express dissimilar tcr repertoires. Eur J Immunol. 2019; 49:398–412.
104. Sage PT, Sharpe AH. The multifaceted functions of follicular regulatory t cells. Curr Opin Immunol. 2020;67:68–74.
105. Linterman MA et al. Foxp3+ follicular regulatory t cells control the germinal center response. Nat Med. 2011; 17:975–982.
106. Shin DS et al. Lung injury induces a polarized immune response by self-antigen-specific cd4(+) foxp3(+) regulatory t cells. Cell Rep. 2023;42:112839.
107. Rosenblum MD, Remedios KA, Abbas AK. Mechanisms of human autoimmunity. J Clin Invest. 2015;125:2228–2233.
108. Heo YW, Jeon JJ, Ha MC, Kim YH, Lee S. Long-term risk of autoimmune and autoinflammatory connective tissue disorders following covid-19. JAMA Dermatol. 2024; 160:1278–1287.
109. Malviya V et al. Regulatory t-cell stability and functional plasticity in health and disease. Immunol Cell Biol. 2023; 101:112–129.
110. Gladstone DE et al. Randomized, double-blinded, placebo-controlled trial of allogeneic cord blood t-regulatory cells for treatment of covid-19 ards. Blood Adv. 2023; 7:3075–3079.
111. Persa E, Balogh A, Sáfrány G, Lumniczky K. The effect of ionizing radiation on regulatory t cells in health and disease. Cancer Lett. 2015;368:252–261.
112. Sheikh A et al. Selective dependence on il-7 for antigen-specific cd8 t cell responses during airway influenza infection. Sci Rep. 2022;12:135.
113. Mock JR et al. Impact of tregs on at2 cell transcriptomes during resolution of ali and contributions of ifn-gamma. Am J Respir Cell Mol Biol. 2020;63:464–477
114. Fisher MJ. Il-6 levels in acute respiratory failure secondary to non-covid-19 viral infection. CHEST Pulm. 2024; 2:100035.
115. Angriman F et al. Interleukin-6 receptor blockade in patients with covid-19: Placing clinical trials into context. Lancet Respir Med. 2021;9:655–664.